Chemical Engineering Science: X 8 (2020) 100082

Contents lists available at ScienceDirect

Chemical Engineering Science: X

journal homepage: www.elsevier.com/locate/cesx

Single drop breakage in turbulent flow: Statistical data analysis

Eirik H. Herø *, Nicolas La Forgia, Jannike Solsvik, Hugo A. Jakobsen

Department of Chemical Engineering, Norwegian University of Science and Technology, Sem Sælandsvei 4, Kjemiblokk 5, 7491 Trondheim, Norway

ARTICLE INFO

Article history:
Received 17 June 2020
Received in revised form 27 August 2020
Accepted 25 September 2020

Keywords:
Breakage
Fluid particle
Turbulence
Statistical analysis
Population balance equation

ABSTRACT

To improve breakage models in the population balance framework, single octanol droplet experiments have been performed in a channel flow and recorded by high-speed camera. The study investigates impact of mother drop size on the breakage time, breakage probability, average number of daughters and the daughter size distribution for known turbulence characteristics. Each breakage event is associated with an individual turbulence level, based on the local flow characteristics. A clearly defined statistical analysis is presented. Using 95% confidence intervals, the precision of each of the determined properties is described quantitatively. Furthermore, the confidence intervals are a tool for determining whether an increased number of experiments will yield a significant increase in the precision, considered against the sources of error. It is found that 35–50 breakage events are sufficient to obtain confidence intervals of desired precision.

1. Introduction

The dispersed phase properties in multiphase flows are of interest for several fields of industry. Some examples of industrial applications of low turbulence level flows are channel or pipe flow, bio- and chemical-reactor flows, as well as phase separation equipment like gravity separators. To determine the separation of a dispersed phase, or to determine the interfacial mass transfer of a system, information on the size distribution of the dispersed phase is critical. The transient breakage phenomenon must be well understood for predictive simulation of such systems. Even so, the knowledge of the turbulent breakage phenomenon is scarce, likely owing to technological limitations and labor intensive experimental procedures.

One simulation tool available for multiphase flow systems is the population balance equation, PBE. There is a need for experiments on single fluid particle breakage in order to improve or validate breakage models within this framework. This need has previously been acknowledged by e.g. Andersson and Andersson (2006b) and Solsvik and Jakobsen (2015). The experimental data is needed on the source term constitutive equations, which are given here as:

- The breakage frequency $b(D_m)$. Which is found through investigating:
  - The breakage time $t_B(D_m)$, which is the time it takes for a drop of size D_m to break.
  - The breakage probability $P_B(D_m)$, which is the probability that a drop of size D_m will break.
- The average number of daughter drops $\nu(D_m)$, which is the average number of drops produced upon the breakup of a drop of size D_m.
- The daughter size distribution function $P_{DSD}(D_m, D_d)$, which is the probability that a drop of size D_d is produced upon breakup of a drop of size D_m.

Here, D_m is the diameter of the mother drop, i.e. the breaking drop, and D_d is the diameter of a daughter drop. In the context of this article, a mother drop may also refer to a drop not breaking. For simplicity, the source term constitutive equations are written as functions of the drop diameters only. Additionally, they may depend on the turbulent kinetic energy dissipation rate, TDR, ϵ, the viscosity, μ, the density, ρ, of each phase, the interfacial tension, γ, and the turbulent kinetic energy, TKE, k, in addition to other parameters.

Experiments on breakage in dense dispersions, in which many fluid particles are investigated simultaneously, are challenging or impossible to use in validation of local breakage functions (Solsvik et al., 2013). Unfortunately, the number of studies on single fluid particle breakage is low. In addition, the use of different experimental setups and different procedures makes it difficult to compare the available experimental data. The studies in the literature vary in the number of considered events, the statistical procedure employed, the turbulence level and the method of determination of the turbulence level. The studies also use different oils as the dispersed phase and use either tap or distilled water

* Corresponding author.
E-mail address: eirik.h.hero@ntnu.no (E.H. Herø).

https://doi.org/10.1016/j.cesx.2020.100082
2590-1400/

Nomenclature

Latin Letters

$\bar{b}$	estimated breakage frequency [1/s]
$\bar{x}$	mean value
$\boldsymbol{r}$	space coordinate vector [m]
$\boldsymbol{v}_r$	velocity vector [m/s]
ΔN	number of breaking drops
ΔN_B	true number of drops breaking
ΔP	Pressure drop [Pa]
$\Delta P_{DSD}\prime$	discrete daughter size distribution function [1/m^3]
$\Delta P_{DSD}*$	dimensionless discrete daughter size distribution function [-]
ΔV_d	daughter size range
$\hat{P}$	true probability of a favorable outcome
AB	separation distance [m]
b	breakage frequency [1/s]
B_B	birth due to breakage [1/(m^3 m s)]
B_D	death due to breakage [1/(m^3 m s)]
c	parameter
c_L	model parameter
$D*$	Dimensionless daughter diameter
$D*_{max}$	dimensionless drop, complimentary to $D*_{min}$ in (24)
$D*_{min}$	dimensionless smallest drop breaking in (24)
D_c	critical diameter [m]
D_d	daughter drop diameter [m]
D_m	mother drop diameter [m]
D_{max}	in (3), largest drop size present [m]
E	energy [J]
E_c	critical energy [J]
E_s	Surface energy [J]
F	hypergeometric function
f_n	number density function [1/(m^3 m)]
h	breakage yield distribution function [1/m]
K	Bessel function
k	turbulent kinetic energy [m^2/s^2]
L	integral length scale [m]
N	number of observations
N	total number of drops
$P*$	estimated probability
P_B	breakage probability
P_{DSD}	daughter size distribution function [1/m]
$P_{DSD}*$	Dimensionless daughter size distribution function
Q	true probability of an unfavorable outcome
r_d	model distance [m]
S	standard deviation
s	function
t	time [s]
t_B	breakage time [s]
T_n	function, n = 1, 2, 3, 4, 5
u_B	characteristic breakup velocity [m/s]
V_d	daughter drop volume [m^3]
V_m	mother drop volume [m^3]
$z_{\alpha/2}$	normal distribution coefficient
Re_λ	Taylor scale Reynolds number
We	Weber number

Greek Letters

α	confidence interval size
β	Komogorov constant
$\Delta\sigma$	surplus stress [Pa/m^2]
ϵ	turbulent energy dissipation rate [m^2/s^3]
η	Kolmogorov micro scale [m]
Γ	gamma function
γ	interfacial tension [N/m]
Λ	dimensionless critical diameter [m]
μ	dynamic viscosity [kg/(m s)]
μ	true mean
ν	average number of daughters
ν	kinematic viscosity, in Section 2.5 [m^2/s]
ω	confidence interval limit
$\overline{\delta u^2}$	second order longitudinal velocity structure function [m^2/s^2]
ρ	fluid density [kg/m^3]
ρ_c	continouos phase density [kg/m^3]
ρ_d	dispersed phase density [kg/m^3]
σ	standard deviation
σ_s	surface restoring stress [Pa/m^2]
σ_t	turbulent stress [Pa/m^2]

Abbreviations

CFD	Computational Fluid Dynamics
PBE	Population Balance Equation
TDR	Turbulent Kinetic Energy Dissipation Rate
TKE	Turbulent Kinetic Energy

for the continuous phase, which results in different fluid and system properties. In particular, both the interpretation of the studies and the comparison between the studies are challenging due to different or unclear definitions of the breakage event. Partly, this is due to a controversy in the literature regarding the breakage event definition. Solsvik et al. (2016a) outlined two definitions of the breakage event. One is the initial breakage definition, in which the breakage event is considered to end at the first fragmentation. This is employed in the studies of Maaß et al. (2011); Maaß and Kraume (2012) and Nachtigall et al. (2016). The other breakage event definition is the breakage cascade definition, in which the breakage event end at the final fragmentation of intermediate daughter drops. The cascade breakage definition is used in the investigation of Solsvik and Jakobsen (2015) and seemingly also in the daughter size distribution investigations of Maaß et al. (2007). The breakage definition employed has a significant impact on the breakage time, the number of daughters and their size distribution, as the cascade breakage definition considers the time after initial breakage.

Furthermore, the studies in literature investigate different phenomena of the breakage event. Galinat et al. (2005) investigated the breakage probability, daughter size distribution and average number of daughters of single oil droplet breakage in an orifice flow. The number of experiments performed is unclear, but at least 50 to 80 drops where observed for each of the twelve flow conditions. These different flow conditions were obtained by changing the orifice opening and the continuous phase velocity. Further, Galinat et al. (2005) used single drops of heptane or heptane colored with red sudan as the dispersed phase, while the continuous phase was tap water. Due to fluctuations in the diameter of the generated mother drop under the same experimental conditions, the mother drops were divided into classes. The mother drop diameters were between 1.5 to 3 mm and the classes had a width of 0.25 mm. From these mother drop diameter groups, groups based on a Weber number was constructed, where the Weber number was expressed as $\mathrm{We} = \Delta P D_m/\gamma$. Here, ΔP is the pressure drop over the orifice, from which the TDR levels can be found to be between 1 and 20 m^2/s^3, depending on the flow condition, while

Table 1
Fluid and system properties reported in previous studies.

Reference	Continuous phase	Dispersed phase	γ x10^{-3} [N/m]	ρ [kg/m^3]	μ x10^{-3} [kg/(m s)]
Galinat et al. (2005)	Tap water			996	0.82
		Heptane	47	683.7	0.45
		Colored heptane	23.6		
Galinat et al. (2007)	Tap water with glycerin			1100	
		Colored heptane	24.4		
Andersson and Andersson (2006a,b)		Dodecane	53	750	1.5
		Octanol	8.5	819	6.5
Maaß et al. (2007) and		Petroleum		760	1.9
Zaccone et al. (2007)	Unspecified water		2		
	Colored water		28		
Maaß et al. (2011) and	Unspecified water				
Maaß and Kraume (2012)		Toluene	32	870	0.55
		Petroleum	38.5	790	0.65
Nachtigall et al. (2016)		Petroleum		760	1.7
	Unspecified water		43.2		
	Water with SDS		5.9		
		Paraffin oil		861	127
	Unspecified water		53.3		
	Water with SDS		8.4		
Solsvik and Jakobsen (2015)	Distilled water				
		Toluene	33	866.7	0.6
		Petroleum	44.5	754	1.14
		n-Dodecane	41.5	745	1.38
		1-Octanol	8.4	822	7.52
Ashar et al. (2018)	Deionized water			988	1
		Rapeseed oil	20	920	70

no TKE values or relations were given. Finally, the results are presented as functions of the Weber number, although the number of experiments within each Weber number group is not given. The breakage probability was also linked directly to the mother drop size for four different flow conditions. No statistical analysis was presented for the daughter size distribution and the breakage probability, but the average number of daughters are presented as average values with standard deviation. Later, Galinat et al. (2007) performed additional experiments with water-glycerin as the continuous phase, and colored heptane as the dispersed phase. 70 experiments where performed for each of the twelve flow conditions, with the TDR level varying between 0.9 and 2.5 m^2/s^3. In the study, the mother drop diameter was between 1.4 to 2.0 mm. No breakage definition was given in either studies by Galinat et al. (2005, 2007). The reported fluid and system properties of all the considered studies can be seen in Table 1 and a simplified overview of selected studies can be seen in Table 2.

Andersson and Andersson (2006a,b) studied single oil dodecane or octanol drop breakage in a static mixer. The continuous phase was water, for which the properties was not specified. In their study, the breakage time was reported as a function of the TDR level, and presented as an average value with standard deviation. However, no further statistical analysis was presented. In addition, the daughter number distribution of dodecane drops was presented for two different TDR levels. For each reported value, approximately 50 breakage events were considered and the mother drop diameter was kept constant at 1 mm [1]. PIV-experiments and Large Eddy Simulation was used to determine the turbulent characteristics. Depending on the continuous phase flow rate, the volume average the TDR levels was found to be $1.13, 3.69$ and 8.54 m^2/s^3, while the TKE level was found to be $17, 37$ and 64 m^2/s^2. Finally, the employed breakage definition is not mentioned.

Maaß et al. (2007) and Zaccone et al. (2007) investigated oil drop breakage in a channel flow with an impeller blade, mimicking stirred tank flow. They investigated the daughter size distribution for different daughter numbers and reported the daughter number distribution. The dispersed phase was petroleum and the continuous phase was an unspecified type of water, with and without coloring by sudan-black. Further, the TDE was determined from CFD simulations with a k-ϵ model, where the local maximum near the impeller was found to be 26.1 m^2/s^3. The TKE was not given. For each of the mother drop diameters $0.56, 1$ and 2 mm, the number of investigated events are given as $284, 503$ and 184. In addition, a required number of events were reported, however, it is not clear what the significance of this number is or how it was determined. Later, Maaß et al. (2011) and Maaß and Kraume (2012) used the same setup to investigate the daughter number distribution and breakage frequency, the latter as breakage time and breakage probability. The mother drops were toluene with diameters of $0.62, 1.0, 2.0$ and 3.0 mm, as well as petroleum drops of $0.54, 0.7, 1.0, 1.3, 1.9$ and 3.1 mm. For each of the mother drop sizes, the number of total events where between ~ 750 and ~ 1320, of which the number of breakage were between ~ 240 and ~ 780. The results on breakage time and breakage probability were presented with average values and standard deviation. Additionally, the development of the mean value with the number of experiments were investigated. This showed that the values were stable, thus there were more than enough experiments performed. Later, and in the same setup, Nachtigall et al. (2016) investigated the breakage time with emphasis on the deformation process. The mother drops where all 1 mm in diameter and either petroleum or paraffin oil, while the continuous phase was either water or water mixed with sodium dodecyl sulfate. The different combinations of dispersed and continuous phases allowed for the impact of the interfacial tension to be investigated. In the study, the number of events with breakage was between 364 and 917, while the total number of events was between 1021 and 1486. Furthermore, the experimental results are presented as whisker-and-box plots, but no further statistical analysis was presented.

Solsvik and Jakobsen (2015) investigated single oil droplet breakage in a stirred tank. In their study, the breakage time was presented as function of the mother drop size, along with the distribution of daughter drop numbers. Toluene, petroleum, n-

[1] Personal communication

Table 2
Overview of selected single drop experimental studies. *Standard deviation is only shown when determining an average value, e.g. not for breakage probability or daughter size distributions.

Reference	Investigated values	Mother Drop Diameter, D_m [mm]	TDR ϵ [m^2/s^3]	Statistical Treatment
Galinat et al. (2005, 2007)	P_B, v, P_{DSD}	1.5–3	~1–20	Average values with standard deviation*
Maaß et al. (2007)	P_{DSD}	0.56–2	26.1	None
Maaß and Kraume (2012)	t_B, P_B	0.54–3.1	~ 2.3–12.3	Analysis of the development in the mean value
Andersson and Andersson (2006a,b)	t_B, v	1	1.13–8.54	Average values with standard deviation*
Solsvik and Jakobsen (2015)	t_B, v	0.6–4.0	1.14	None
Ashar et al. (2018)	P_B, v	0.07–0.55	535–2480	Average values with uncertainty

dodecane and 1-octanol was used as the dispersed phase and distilled water was used as the continuous phase. The diameter of the mother drops was varying between 0.6 to 4 mm, and thus divided into groups with a width of 0.5 mm. There were between 180 to 250 breakage events for each oil, but greatly varying in numbers within each mother drop group. Here, the number of breakage events were between 1 and 71. The TDR level was determined from the power input and given as a volume average of the entire tank, at 1.14 m^2/s^3. No information on the TKE was given. Furthermore, no statistical method was presented.

Ashar et al. (2018) studied single droplet breakage in a stirred tank and investigated the breakage probability and the average number of daughters. The results were reported as functions of a turbulent Weber number and presented as average values with uncertainty. However, the statistical procedure was not given. A deformation time was also presented, which was defined as the time from turbulent vortex interaction until the maximum deformation. This is believed to be the time of energy transfer from the turbulent vortex to the breaking drop. As this maximum deformation occurs at an earlier time instance than the instance of first fragmentation, the deformation time is shorter than the initial breakage time. While not explicitly defined, the daughter number appears to be calculated according to the cascade breakage definition. In the study, the mother drops were rapeseed oil drops with a diameter between 0.07 and 0.55 mm, and deionized water was used as the continuous phase. In total, 285 breakage events were investigated for two different TDR levels, 535 and 2480 m^2/s^3. The TDR level was determined from a procedure arising from PIV analysis, and given as a local average value of the volume near the impeller. The TKE is not given.

Although it may initially appear otherwise, the studies presented above follow a similar procedure when reporting their results. An investigated parameter, e.g. breakage probability, is plotted against another variable, e.g. mother drop diameter. The other variables are assumed constant, where the TDR level is taken to be that of the single phase flow field of the continuous phase. It should be noted that when reporting the results by Weber number instead of the drop diameter, it is not possible to regain the dependency on ϵ and D_m, except if either ϵ or D_m is kept constant. Thus, the data cannot be used to validate most of the currently available models.

Based on the studies presented here, some generalizations of the status of single fluid particle breakage investigations are possible. Firstly, no investigation covers all of the information needed to model the terms in the PBE. That is, information on the breakage frequency, b, average number of daughters, v, and daughter size distribution, P_{DSD}, have not all simultaneously been extracted from the same experimental data set. Consequently, subsequent model validation must rely on experimental data from different experimental setups and procedures, a strategy which does not ensure consistency.

Second, most of the previous studies employ a volume average TDR level, while the breakage models are developed considering local turbulence characteristics. The regions of breakage in the employed experimental facilities have large gradients in the turbulence level, thus the difference in local and average turbulence level may be significant. In turn, the reported turbulence characteristics may not be sufficiently accurate to represent the turbulence characteristics responsible for the breakage event. Additionally, there are two other weaknesses related to the flow conditions. Weakness one, the regions of breakage have a significant presence of mean flow shear, which possible impact on the breakage cannot be distinguished from the impact of the level of turbulence. Weakness two, no value of the TKE is associated with the breakage. Thus, the impact of the entire range of turbulence cannot be computed, only the impact of the inertial subrange of turbulence. How to model the entire range of turbulence has been shown by Solsvik and Jakobsen (2016a), and a summary is shown in Section 2.5.

Finally, the studies commonly presented the determined average value with a standard deviation, and no clear statistical analysis is available. As experimental procedures are subject to many sources of error, the statistical analysis, along with a discussion on uncertainty, is important in regards to the accuracy and precision of the results. Accuracy and precision are considered to be different concepts within uncertainty analysis, and the difference is shown graphically in Fig. 1. If measurements are repeated, a high accuracy yields values that are near the true value, while a high precision yields nearly the same value from each measurement. The statistical analysis, when resulting in a 95% confidence interval, is a tool for describing the precision of the data. However, it does not address the accuracy. This can be better understood by considering the plausible errors sources, which are usually divided into random errors and systematic errors. Random errors are largely due to changing initial conditions between each experiment. As the name implies, random errors are considered to be randomly applied. Systematic errors, on the other hand, arise from the experimental procedure and assumptions, and are generally not considered to be randomly applied. In a simplified view, the random errors may be assumed to be accounted for by the statistical analysis, while the systematic errors are not accounted for. Thus, systematic errors may skew the data in such a way that the confidence interval does not contain the true value. That is, while the experimentally determined value may be precise, it does not need to be accurate. It is possible to account for systematic errors if the impact on the results is known and quantified. Unfortunately, quantification of the systematic errors is rarely possible in complex experimental procedures. Nevertheless, performing a statistical analysis is particularly important due to the labor intensive

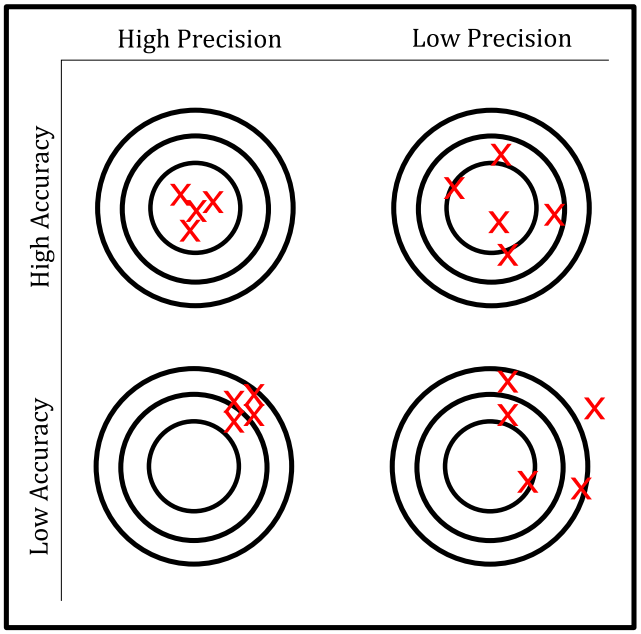

Fig. 1. The difference between accurate and precise experimental techniques.

methodology of the state of the art single droplet breakage experiments. The gain in precision from additional experiments must be considered against the increased workload. An increased number of experiments may lead to only a small increase in the precision, but may lead to additional aspects of the breakage phenomenon not being investigated. This may be part of the reason that no investigation covers all the information needed to model the source term constitutive equations in the PBE.

The purpose of this work is to obtain data on and elucidate the breakage phenomenon in general, and the impact of mother drop size in particular. An experimental facility has been constructed with a design that offers low gradients in the turbulence level of the continuous phase. As the local turbulence level is known, due to the investigation by La Forgia et al. (2018), each breakage event may be associated with relevant and local turbulent characteristics. This allows for a quantified difference in turbulence level between investigated events. Furthermore, the design allows for video capture of the entire breakage event, such that the videos may be investigated according to the procedure outlined in Herø et al. (2019). The resulting data should be consistent, as the breakage frequency, b, the average number of daughters, ν, and the daughter size distribution P_{DSD} are determined from the same events. Furthermore, this study employs a transparent statistical methodology as a tool to discuss the precision of the data. This statistical procedure is also used to identify whether additional experiments are beneficial.

2. Turbulent breakage models

The PBE is a common and powerful simulation tool. It is a framework that dynamically describes the change in the number density distribution of the dispersed phase (Ramkrishna, 2000). Simplified to consider only accumulation, convection and breakup, the PBE in terms of the number density function, f_n, can be written as (Jakobsen, 2014)

$$\frac{\partial f_n(D_m,\boldsymbol{r},t)}{\partial t}+\nabla\cdot[\boldsymbol{v}_r(\boldsymbol{r},D_m,t)f_n(D_m,\boldsymbol{r},t)] = -B_D(D_m,\boldsymbol{r},t)+B_B(D_m,\boldsymbol{r},t) \quad (1)$$

$$B_D(D_m)=b(D_m)f_n(D_m) \quad (2)$$

$$B_B(D_m)=\int_{D_m}^{D_{max}}\nu P_{DSD}(D_m,D_d)b(D_d)f_n(D_d)dD_d \quad (3)$$

Here, $\boldsymbol{r}$ is the space coordinate vector, t is the time, $\boldsymbol{v}_r$ is the velocity vector and D_m and D_d are denoting the drop diameters of the mother and daughter drop. Further, b is the breakage frequency, ν is the average number of daughter particles and P_{DSD} is the daughter size distribution function. The two latter quantities may be combined to the breakage yield redistribution function, h. Finally, the terms on the right hand side of (1) are the sink and source terms that represent the breakage death, (2), and breakage birth of drops, (3), of diameter D_m due to breakage events.

In order to use the PBE in simulations, e.g. coupled with computational fluid dynamics, the terms of (2) and (3) must be modeled. If experimental data are to improve these models, it is critical to consider how the models are developed. The mechanisms considered and the model interpretation of the breakage phenomenon should coincide with the interpretation of the data from physical experiments. Thus, two classic and commonly used models are presented in this section.

2.1. Coulaloglou and Tavlarides

In developing their model, Coulaloglou and Tavlarides (1977) assumed a drop would break due to local pressure fluctuations only. Further, they assumed binary breakage, locally isotropic turbulence and that the size of the droplet diameter falls within in the inertial subrange of turbulence. The basic assumption is that a breakup occurs if a drop collides with a turbulent eddy of sufficient energy. The breakage frequency, $b(D_m)$, which is required in both (2) and (3), is determined as the reciprocal of a breakage time, $t_B(D_m)$, multiplied by the fraction of drops breaking, $\frac{\Delta N(D_m)}{N(D_m)}$. This fraction of drops breaking is interpreted as the breakage probability $P_B(D_m)$, i.e. the probability that a drop will break. Thus, the breakage frequency relation becomes

$$b(D_m)=\frac{1}{t_B(D_m)}\frac{\Delta N(D_m)}{N(D_m)}=\frac{1}{t_B(D_m)}P_B(D_m) \quad (4)$$

The breakage probability is assumed proportional to the fraction of the turbulent eddies that collides with the drop, where the energy of the turbulent eddy is larger than the drop surface energy. Further, this fraction of turbulent eddies is assumed to be described by the Maxwell–Boltzmann 2D energy distribution, thus

$$P_B(D_m)=\int_{E_c(D_m)}^{\infty}P(E(D_m))dE=\exp\left(-\frac{E_c(D_m)}{E(D_m)}\right) \quad (5)$$

in which $E(D_m)$ is the turbulent energy associated with eddies of size D_m and $E_c(D_m)$ is the critical value that the turbulent energy $E(D_m)$ must overcome. $E_c(D_m)$ is taken as the surface energy

$$E_c(D_m)\propto\gamma D_m^2 \quad (6)$$

in which γ is the interfacial tension and D_m is the diameter of the drop. The energy of the turbulent eddies is taken to be

$$E(D_m)\propto\rho_d D_m^3\overline{\delta u^2}(D_m) \quad (7)$$

where ρ_d is the density of the dispersed phase. The second order longitudinal velocity structure function, $\overline{\delta u^2}(D_m)$, is determined from Kolmogorov theory

$$\overline{\delta u^2}(D_m)=\overline{|u(r+D_m,t)-u(r,t)|^2}=\beta(\epsilon D_m)^{2/3} \quad (8)$$

Thus, inserting (6) and (7) in (5) the expression becomes

$$P_B(D_m) = \exp\left(-\frac{c_1\gamma}{\rho_d\epsilon^{2/3}D_m^{5/3}}\right) \tag{9}$$

in which c_1 is a parameter. The breakage time was estimated by assuming the eventual centers of mass of the daughter drops behave like two turbulent eddies. If AB is the initial separation distance, the separation distance $AB\prime$ of the two masses at time t are given as

$$[AB\prime(t)]^2 \propto (AB\ \epsilon)^{2/3}t^2 \tag{10}$$

Further, if both AB and the distance at breakage are proportional to the mother drop diameter, the equation can be solved for t_B as

$$t_B(D_m) = c_2 D_m^{2/3}\epsilon^{-1/3} \tag{11}$$

in which c_2 is a parameter. Finally, the breakage frequency was determined from (4) by combining expressions for the breakage time, (11), and the fraction of drops breaking, (9)

$$b(D_m) = c_2^{-1}D_m^{-2/3}\epsilon^{1/3}\exp\left(-\frac{c_1\gamma}{\rho_d\epsilon^{2/3}D_m^{5/3}}\right) \tag{12}$$

In the source term, (3), two additional functions are required; the average number of daughters, ν, and the daughter size distribution function, $P_{DSD}(D_m, D_d)$. As aforementioned, binary breakage is assumed, thus the average number of daughters are known. Further, the daughter size distribution function is assumed to fit a normal distribution in which the variance is set so that $> 99.6\%$of droplets formed lie in the volume range 0 to D_m. The resulting normal distribution has a maximum for equal sized daughter drops and a low probability for a significant size difference. In terms of diameter the expression becomes (Solsvik et al., 2013)

$$P_{DSD}(D_m, D_d) = \frac{2.4}{D_m^3}\exp\left(-\frac{4.5\left(2D_d^3 - D_m^3\right)^2}{D_m^6}\right)3D_d^2 \tag{13}$$

While in terms of volume, the expression becomes (Coulaloglou and Tavlarides, 1977)

$$P_{DSD}(V_m, V_d) = \frac{2.4}{V_m}\exp\left(-\frac{4.5(2V_d - V_m)^2}{V_m^2}\right) \tag{14}$$

2.2. Martinez-Bazan et al.

The Martínez-Bazán et al. (1999a,b) breakage frequency model represents a novel attempt to represent the fluid particle-turbulence interaction in terms of the directly measurable turbulent stress quantity, i.e. the second order structure function. Most of the predecessor breakage frequency models rely on the more abstract drop-eddy collision or interactions frequencies which are difficult to validate due to the vague definition of the eddy concept. The MB model avoids the eddy concept. Thus, the model may be considered more fundamental in nature. In developing their model, Martínez-Bazán et al. (1999a,b) assumed that a bubble deforms and breaks if the turbulent stresses of the surrounding fluid flow is sufficiently large. That is, this stress, σ_t, has to be at least larger than the bubble surface restoring stress, σ_s. They assumed locally isotropic turbulence, that the bubble diameter falls within the inertial subrange of turbulence, and binary breakage. As such, the model shares similarities with the model of Coulaloglou and Tavlarides (1977). The breakage frequency is given as

$$b(D_m) \propto \frac{1}{t_B(D_m)} \tag{15}$$

that is, compared to Coulaloglou and Tavlarides (1977), the breakage frequency is purely determined from the inverse of an expression for breakage time. This breakage time is defined as

$$t_B(D_m) \propto \frac{D_m}{u_B} \tag{16}$$

in which D_m is the bubble size and u_B is a characteristic breakup velocity. This velocity is assumed proportional to the square root of the difference between the turbulent stress, σ_t and the bubble surface restoring stress σ_s as

$$u_B \propto \sqrt{\sigma_t - \sigma_s} \tag{17}$$

in which σ_t is found as

$$\sigma_t = 1/2\rho_c\overline{\delta u^2}(D_m) = 1/2\rho_c\beta(\epsilon D_m)^{2/3} \tag{18}$$

where ρ_c is the density of the continuous phase. Further, σ_s is found as

$$\sigma_s = \frac{6E_s(D_m)}{\pi D_m^3} = 6\frac{\gamma}{D_m} \tag{19}$$

where $E_s(D_m)$ is the surface energy defined as $E_c(D_m) = \pi\gamma D_m^2$. Thus, the expression for the breakage time becomes:

$$t_B(D_m) \propto \frac{D_m}{\sqrt{\beta(\epsilon D_m)^{2/3} - 12\gamma/(\rho_c D_m)}} \tag{20}$$

and finally the expression for breakage frequency becomes:

$$b(D_m) = c_3\frac{\sqrt{\beta(\epsilon D_m)^{2/3} - 12\gamma/(\rho_c D_m)}}{D_m} \tag{21}$$

In the event that the bubble surface restoring stress, σ_s, is larger or equal to the turbulent stress, σ_t, breakup is assumed not to occur and the breakage frequency is set to zero. Thus, for a given system there is a critical diameter, D_c, where the bubble surface stress is equal to the turbulent stress. From (18) and (19)

$$D_c = \left(\frac{12\gamma}{\beta\rho_c}\right)^{3/5}\epsilon^{-2/5} \tag{22}$$

Due to the assumption of binary breakage the only remaining expression required in (3) is the daughter size distribution function, P_{DSD}. Martínez-Bazán et al. (1999a,b) postulated that the probability of forming two bubbles of diameter $D_{d,1}$ and $D_{d,2}$ is weighted by the product of the surplus stress associated with the diameters $D_{d,1}$ and $D_{d,2}$, defined as

$$\Delta\sigma(D_{d,n}) = \frac{1}{2}\rho_c\beta(\epsilon D_{d,n})^{2/3} - 6\gamma/D_m \tag{23}$$

in which n is either 1 or 2 and D_m is the diameter of the mother bubble. If a bubble of diameter $D_{d,1}$ is formed, the diameter of the second bubble is given from volume conservation. The original daughter size distribution function was not volume conserving, thus it was later updated by Martínez-Bazán et al. (2010). Written in dimensionless form, such that $P^*_{DSD}(1, D^*)\cdot D_m = P_{DSD}(D_m, D_d)$, the updated daughter size distribution function is given as

$$P^*_{DSD}(1, D^*) = \frac{D^{*2}\left[D^{*2/3} - \Lambda^{5/3}\right]\left[\left(1 - D^{*3}\right)^{2/9} - \Lambda^{5/3}\right]}{\int_{D^*_{min}}^{D^*_{max}} D^{*2}\left[D^{*2/3} - \Lambda^{5/3}\right]\left[\left(1 - D^{*3}\right)^{2/9} - \Lambda^{5/3}\right]dD^*} \tag{24}$$

in which $D^* = D_d/D_m$and $\Lambda = D_c/D_m$. The minimum diameter, D_{min}, is the smallest diameter of a daughter bubble for which the turbulent stress is equal to the restoring surface pressure, i.e. $\sigma_t(D_{min}) = \sigma_s(D_{min})$. The maximum diameter, D_{max}, is the complimentary diameter that conserves the mass of the mother bubble. From this, the dimensionless quantities are obtained as $D^*_{max} = D_{max}/D_m$ and $D^*_{min} = D_{min}/D_m$. The resulting daughter size distribution function behave similarly to the model of Coulaloglou and

Tavlarides (1977) in which equal sizes daughters are the most likely outcome of a breakage event.

The model of Martínez-Bazán et al. (1999a,b, 2010) were originally designed considering very high Reynolds number flows, thus breakage was frequent and $P_B(D_m) \sim 1$. Solsvik et al. (2017) suggested to add a breakage probability to the breakage frequency, analogous to the model of Coulaloglou and Tavlarides (1977), in order to expand the model to be valid also for lower Reynolds number flows. The breakage probability was defined as a shifted version of (5):

$$P_B(D_m) = \exp\left(-\frac{E_c(D_m - D_c)}{E(D_m - D_c)}\right) \tag{25}$$

in which E_c and E are defined by (6) and (7), respectively. For bubbles smaller than the critical diameter D_c, the breakage probability was set to zero.

The model of Martínez-Bazán et al. (1999a,b, 2010) was originally designed considering a gas–liquid system. Later, Eastwood et al. (2004) investigated liquid–liquid breakage in the same experimental setup. They found that the breakage frequency was underpredicted for fluid particles with non-negligible density and viscosity at low Weber numbers. However, model adaptions, e.g. Revuelta et al. (2006) and Solsvik et al. (2013), have been found to provide good agreement with data from liquid–liquid experiments. Some examples can be seen in the appendix of Solsvik et al. (2013).

2.3. Model constraints

In the models of Coulaloglou and Tavlarides (1977) and Martínez-Bazán et al. (1999a,b, 2010) the breakage frequency goes trough a maximum for increasing mother drop diameter. This behavior was criticized by for example Tsouris and Tavlarides (1994), who argued that the breakage frequency should increase monotonously. Later, experimental data have suggested that this maximum is possible, e.g. Maaß and Kraume (2012). Subsequently, the behavior of the breakage frequency is still a matter of debate. Further, both the model of Coulaloglou and Tavlarides (1977) and the model of Martínez-Bazán et al. (1999a,b, 2010) assume binary breakage. As this assumption is possibly erroneous, other authors have considered a different average number of daughters in their model derivations, e.g. Konno et al. (1983) and Han et al. (2011, 2013, 2015). Of particular interest is the framework proposed by Diemer and Olson (2002) which allows for any average number of daughters, also non-integers. The main drawbacks of the framework are the prediction of equal sized daughters, which might be erroneous, and the need for fitting of model parameters to the specific system in order to be volume and number conserving.

In the available frameworks, the average number of daughters, ν, needs to be known a priori in order to design the daughter size distribution function, P_{DSD}. The constraints on the daughter size distribution function must satisfy the normality or number conservation condition

$$\int_0^{D_m} P_{DSD}(D_m, D_d) dD_d = 1 \tag{26}$$

I.e. all daughters exists in the interval $[0, D_m]$. Further, the breakage yield redistribution function, $h(D_m, D_d) = \nu P_{DSD}(D_m, D_d)$, should be volume conserving;

$$\int_0^{D_m} D_d^3 h(D_m, D_d) dD_d = D_m^3 \tag{27}$$

which is mass conserving given constant density.

2.4. Other models

Several adaptations of the model of Coulaloglou and Tavlarides (1977)(e.g. Konno et al., 1983; Vankova et al., 2007; Maaß and Kraume, 2012) and the model of Martínez-Bazán et al. (1999a,b, 2010)(e.g. Håkansson et al., 2009; Solsvik et al., 2013) exist. While the models change parameters values, add some criteria for breakage or otherwise modify the originally proposed models, they do not change the concepts and breakage event definition. Thus, the experimental data needed for validation of the original models proposed by Coulaloglou and Tavlarides (1977) and Martínez-Bazán et al. (1999a,b, 2010) may also be used for validation of the adapted models.

Furthermore, another group of models within the PBM framework exists. Instead of (1), the PBM is formulated considering sections of the internal coordinate, in what is often referred to sectional models. Of particular relevance are the models proposed by Luo and Svendsen (1996) and Andersson and Andersson (2006b), and recently Xing et al. (2015) and Liao et al. (2018). Special care should be taken as to what framework the models are based on as the models are not directly interchangeable. While the models are possible to reformulate, the procedure is not trivial. Interested readers are referred to Lasheras et al. (2002), Mitre et al. (2010) or Solsvik et al. (2013). However, the if more fundamental form of the breakage frequency, b, average number of daughters, ν, and daughter size distribution P_{DSD} are investigated experimentally, the results can be used in validating models of both frameworks.

Reviews of most of the available breakage models have been published by Lasheras et al. (2002), Liao and Lucas (2009) and Solsvik et al. (2013).

2.5. Coulaloglou and Tavlarides in the entire range of the turbulence spectrum

Recently, some authors (e.g. Solsvik and Jakobsen, 2016a,b; Solsvik et al. 2017; Karimi and Andersson, 2018, 2019) have presented methods to expand several models from only considering the inertial subrange of turbulence, into considering the entire range of the turbulence spectrum. This change in modeling of turbulent stress is of critical importance when comparing model results with experimental data, in particular when the droplet size falls outside of the inertial subrange of turbulence.

Solsvik and Jakobsen (2016a) showed that the model of Coulaloglou and Tavlarides (1977) could be expanded to consider the full range of turbulence. First, they recognized that the expression for breakage time, (11), could be written as

$$t_B(D_m) = c_4 \frac{D_m}{\sqrt{\overline{\delta u^2}}(D_m)} \tag{28}$$

Thus, the breakage time depends on the expression for the second order longitudinal structure function. The expression for breakage probability, (9), already depend on the second order longitudinal structure function through (7). Similarly, the resulting expression for breakage probability becomes

$$P_B(D_m) = \exp\left(-\frac{c_5 \gamma}{\rho_d D_m \overline{\delta u^2}(D_m)}\right) \tag{29}$$

Thus, the expressions for breakage time and breakage probability, and subsequently the breakage frequency, can be expanded to be valid for the entire range of turbulence if the expression for the second order longitudinal structure function is valid in the entire range of turbulence. Such an expression can be given as, Solsvik and Jakobsen (2016b),

$$\overline{\delta u^2}(D_m) = \frac{4}{3}k\left(\frac{D_m^2}{r_d^2 + D_m^2}\right)^{2/3} \cdot (1 - [T_1(D_m) + T_2(T_3(D_m)T_4(D_m) - T_5(D_m))]) \quad (30)$$

where k is the TKE and r_d is given by

$$r_d = (15\beta)^{3/4}\eta \quad (31)$$

where β is the Kolmogorov constant and $\eta = (\nu/\epsilon)^{1/4}$ is the Kolmogorov micro scale, in which ν is the kinematic viscosity. The different T_n expressions are given as:

$$T_1(D_m) = \frac{2}{[s(D_m)]^2}F\left(\left(-\frac{1}{3}\right)^{\frac{1}{2}}, \left(\frac{3}{2}\right)\middle| \frac{[s(D_m)]^2}{4}\right) \quad (32)$$

$$T_2 = 3^{3/2}\Gamma\left(\frac{2}{3}\right) \quad (33)$$

$$T_3(D_m) = 27 \cdot 2^{1/3}[s(D_m)]^{2/3}\Gamma\left(\frac{2}{3}\right) \quad (34)$$

$$T_4(D_m) = \frac{1}{352\pi}F\left(\left(\frac{7}{3}\right)^{\frac{11}{6}}, \left(\frac{17}{6}\right)\middle| \frac{[s(D_m)]^2}{4}\right) \quad (35)$$

$$T_5(D_m) = \frac{2^{2/3}}{2\pi[s(D_m)]^{2/3}}K_{\frac{4}{3}}(s(D_m)) \quad (36)$$

in which F is the hypergeometric function, K is the Bessel function and Γ is the gamma function. Further,

$$s(D_m) = D_m/\left(c_L^{-1/2}L\right) \quad (37)$$

where c_L is a model parameter value which can be estimated from, Solsvik (2017),

$$c_L(\mathrm{Re}_\lambda) = \exp\left[-\frac{4.478 + 18.362\beta}{\mathrm{Re}_\lambda^{1.075-0.070\beta}}\right] - 1.913 + 2.169\beta \quad (38)$$

Finally, $L = \frac{k^{3/2}}{\epsilon}$ is the integral length scale and Re_λ is the Taylor scale Reynolds number given as;

$$\mathrm{Re}_\lambda = \sqrt{\frac{20}{3}\frac{k^2}{\epsilon\nu}} \quad (39)$$

3. Experimental setup and procedure

An experimental facility has been constructed to investigate turbulent breakage of oil droplets in water, as previously described in La Forgia et al. (2018) and Herøet al. (2019). The facility is constructed as a loop, as can be seen from Fig. 2. A pump (numbered 2 in the sketch) is placed downstream from a water tank (1) and upstream of a droplet generation section 4. In the droplet generation section, a single oil droplet can be produced, which travels downstream into the main test section (7), or breakage section. In the end, the water and oil drop return to the tank, which also serves as a gravity separator.

The breakage section consists of a square vertical channel in which droplets may be observed by two cameras (6). To facilitate this observation, the channel consists of two glass walls. The two remaining walls have periodic rods in order to increase the turbulence level. The channel itself is 1 m long and has a cross-sectional area of 30 mm x 30 mm. The rods have a cross-sectional area of 3 mm x 3 mm and are placed every 10 mm in the channel. The resulting flow pattern and turbulence level has been investigated using laser doppler velocimetry in La Forgia et al. (2018). In the droplet generation section, downstream of the breakage section, single spherical 1-octanol (Sigma–Aldrich, product number 472328) droplets are generated from a glass cannula connected to a syringe pump (5) of the type KDS Legato 180. The oil is dyed with Sudan Black B (RAL Diagnostics) and the resulting properties are density $\rho = 825$ kg/m^3, dynamic viscosity $\mu = 9.09 \cdot 10^{-3}$ kg/(m s) and interfacial tension $\gamma = 8.20$mN/m. The continuous phase is clean reverse-osmosis water, where the water pump of type MDL-0670 from SPX Flow Technology provides an area average velocity of 1 m/s.

The two cameras are of the type Photron FASTCAM Mini AX100 540 K M3, which have a maximum resolution of 1024 x 1024, which is only fully used in one direction. The two cameras record from 40 mm to 400 mm above the channel entry for a total section length of 360 mm, i.e. the full channel length is not recorded. Further, the two cameras are connected and synchronized in time. The resulting images are overlapping in a small area and semi-automatically converted to one image through MATLAB. The resolution gives the pixel size as 0.175 mm by 0.175 mm, thus a drop at 1 mm diameter has almost 6 pixels covering its diameter. Moving with a speed of 1 m/s, the centroid of a drop moves 0.25 mm, or ~ 1.4 pixel side lengths, between two frames. The cameras records at 4000 frames per second and this high framerate is beneficial on several accounts. Firstly, the accuracy of the determined breakage times is dependent on the frame rate. Secondly, the average number of daughters and the daughter size distribution in the initial breakage definition can only be accurately determined at high framerates. Solsvik et al. (2016a) showed that the number of daughters in the initial breakage definition was tending towards two for increasing framerate. However, their setup did not allow for more than 1450 frames per second, which was not enough to discern exactly two daughters per breakage. Finally, post processing the images automatically is simpler when the drops travel a short distance between the frames. There is often a trade-off between the resolution selected and the framerate of the camera. In the current study, the framerate at maximum resolution was considered sufficient for the accuracy required. At this framerate, the initial breakage definition always results in two daughters. Thus, the tradeoff between framerate and resolution has not been further analyzed.

Three LED lamps, of the type Multiled LT-V9-15 by GS Vitec, provide the illumination required. The lamps are run continuously, i.e. not synchronized with the cameras. The light is diffused by opaque paper in order to obtain a more even light distribution.

The size of the droplet generated in the generation section is dependent on cannula tip surface area and the continuous flow past the cannula tip. Due to fluctuations in the latter, the droplets are generated with some variation in their size. Such behavior has previously been reported in comparable setups, e.g. Galinat et al. (2005) and Maaß et al. (2009). Due to this fluctuation in size, it was in the present work necessary to divide the experimental data into four size groups based on the mother drop diameter after the experiments have been performed. In this way, the impact of mother drop size on breakage time, t_B, breakage probability, P_B, average number of daughters, ν, and the daughter size distribution P_{DSD}, can be investigated. As such, the standard deviation is not as much an error as it is a measurement of how similar the grouped drops are. As the smallest drop sizes are most difficult to produce consistently, as well as the drops that have the lowest breakage probability, this group is made with the largest size range. The resulting mean diameter and number of events of each group can be seen in Table 3. As the number of breakage events are different in each mother drop size group, the impact of this number on the statistical precision can be investigated. Furthermore, the number of breakage events are comparable to the studies discussed in Section 1.

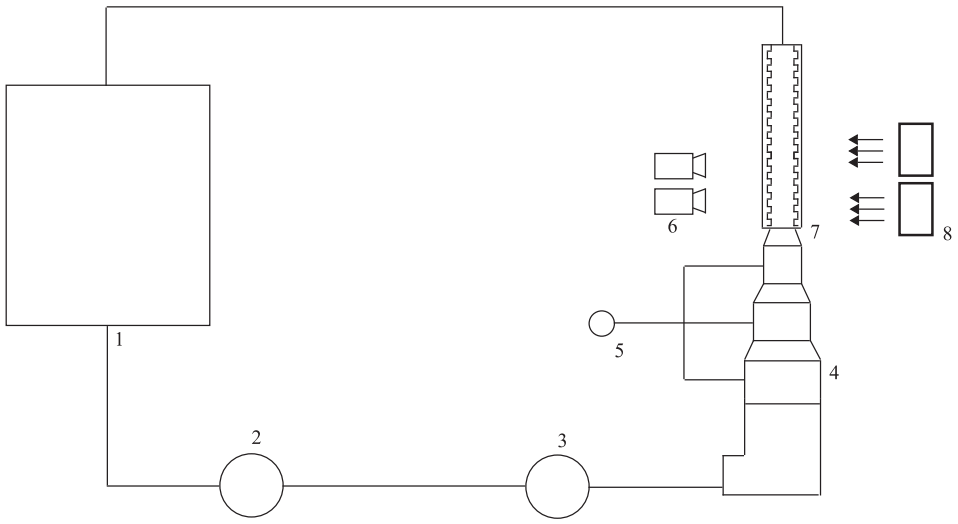

Fig. 2. Schematic drawing of the experimental setup. 1. Water tank and phase separator, 2. water pump, 3. flow meter, 4. droplet generation section, 5. oil syringe pump, 6. two cameras, 7. breakage section, 8. illumination.

All events are interpreted through both initial breakage definition and cascade breakage definition, as outlined in the following Sections 3.1 and 3.2. Thus, two sets of interpreted data are produced from the same experimental raw data. In order to discriminate between breakup in the center of the channel and the high shear region near the walls, a region of wall breakage is defined as drops breaking with their centroid within a horizontal distance of 1.5 mm from the tip of a rod. The value of 1.5 mm is an estimation based on two criteria. Mainly, a distance of 1.5 mm is 5% of the channel width. Thus, the two regions, one on each side of the channel, cover a total of 10% of the channel. Additionally, a spherical drop with its centroid at the 1.5 mm line would not touch the baffle, unless the drop is 3 mm or larger in diameter. Drops of this size is much larger than the biggest drops considered in this study. The breakage events in this region are not included in the data, as the number of events were too few and the impact of shear forces on the breakage events cannot be discerned from that of the turbulence level. When interpreting an event through the cascade breakage definition some daughter drops may enter the wall breakage region. In this case, any proceeding breakups of this particular daughter are not considered to be part of the breakage event. The event is otherwise interpreted following the proposed procedure. Similarly, when a deformed daughter drop leave the field of view, the breakage event is assumed to have ended for this daughter.

3.1. Image analysis

The procedure for extracting data from high speed videos have been described in detail by Herøet al. (2019). In this work, the procedure is employed with a minor modification in the determination of daughter drop sizes. This difference is described and discussed further in Section 4.9, in which a short discussion on the determination of the breakage event start is included. The procedure may be outlined as follows. Each frame of the high speed video is subtracted an image in which there is no drop and the resulting image is converted to a binary image by a gray-level threshold. From the pixels of the binary image, the position, sizes and number of drops in each image can be found. The procedure is implemented and performed in MATLAB, requiring substantial manual input.

The image analysis considers both the initial breakage definition and the cascade breakage definition. First, the start and end instances of the breakage event must be determined;

- Breakage event start is when a spherical mother drop starts to deform, and this deformation process is directly related to a fragmentation of the drop.
- Breakage event end for the initial breakage definition is when the mother drop fragments.
- Breakage event end for the cascade breakage definition is when the final intermediary daughter fragments.

When these two instances are known for a breakage event, the breakage time can be computed as the time period between them. The number of daughters and their sizes are found at the breakage end instance. The TDR level is assumed equal to that of the continuous phase. This TDR level has previously been determined by laser doppler velocimetry, see La Forgia et al. (2018), such that each position of the channel is associated with a local turbulence level. In the case of breakage, the TDR level is taken to be that of the position at breakage start. Thus, it is assumed that a single turbulent vortex-drop interaction is occurring at this position and time instance. For the cases where the drop did not break, the TDR level is taken as the maximum TDR level along the recorded drop path.

It is noted that, by the breakage event definitions applied in this study, the breakage end instance is not an equilibrium state. Both broken and unbroken drops may break, in new independent breakage events, after leaving the test section.

As an example of the breakage definitions applied, Fig. 3 shows an image sequence of a binary breakage, in which a mother drop is broken into two unequal sized drops. In this case the end criteria of the initial breakage definition and cascade breakage definitions coincide, and subsequently the determined breakage time, daughter number and daughter sizes are equal.

Table 3
Mother diameter with standard deviation and number of events investigated.

Mother diameter [mm]	Total number of events	Number of events with breakage
1.0 ± 0.2	284	35
1.48 ± 0.08	379	115
1.87 ± 0.05	148	53
2.23 ± 0.06	154	83

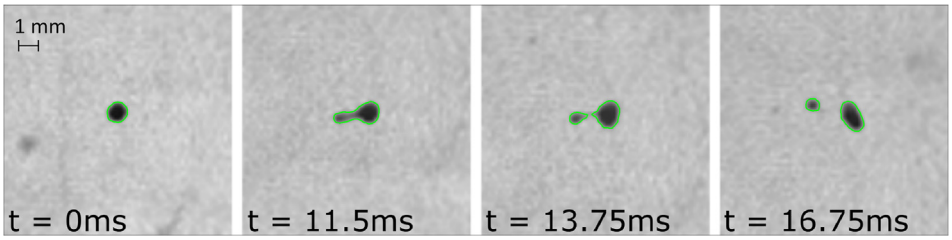

Fig. 3. Binary breakup resulting in two daughters of different size. The mother drop was 0.91 mm in diameter.

Conversely, Fig. 4 shows an example of a sequence of breakups. The initial mother drop is deformed with a long thin thread between two forming daughters, this thread later breaking up into several small daughters. In turn, as the two breakage event definitions differ in the interpretation of the end instance, the resulting breakage time, daughter number and daughter size distribution are different. It should be noted that the two definitions always coincide with regard to the breakage probability.

For completeness, Fig. 5 shows an equal sized breakage, which is a common outcome of the experiments. As above, the two breakage definitions differ in the interpretation of the end instance. In the interpretation according to the initial breakage definition, there are two near equal sized droplets. In the cascade breakage definition, there are still two near equal sized daughters, but also an additional small droplet.

3.2. Interpretation of image analysis data

After the individual videos have been analyzed, the breakage time, t_B, breakage probability, P_B, average number of daughters, ν, and the daughter size distribution P_{DSD} must be determined from the resulting set of data. In this study, these values are determined for each of the mother size groups seen in Table 3. The breakage time is found as the average value of all the drops breaking, while the breakage probability is determined from the fraction of drops breaking to the total number of drops in the mother size group, also those not breaking. Afterwards, the determined breakage time and breakage probability values are combined to the breakage frequency according to (4), i.e. the breakage frequency is not explicitly determined. The number of daughter particles are found as the average number of daughters that are produced from the breakage events of the corresponding mother drop size group. Thus, in this procedure, the breakage time, the breakage probability and the number of daughter particles are a single average value for each mother drop size group. The procedure of obtaining the daughter size distribution function from the experimental data set is not immediately obvious. The first step is to approximate the probability of a daughter appearing in a particular daughter size range with a width of ΔV_d;

$$\Delta P^*_{DSD}(V_m, V_d) = \frac{\text{Number of particles in range}[V_d - \Delta V_d/2,\ V_d + \Delta V_d/2]}{\text{Total number of particles in range}[0,\ V_m]} \tag{40}$$

Following this procedure, the discrete variable $\Delta P^*_{DSD}(V_m, V_d)$ should sum to one. In order to fulfill the constraints in Section 2.3, (40) must be divided by the daughter size range, ΔV_d to obtain another discrete function, $\Delta P\prime_{DSD}(V_m, V_d)$;

$$\Delta P\prime_{DSD}(V_m, V_d) = \Delta P^*_{DSD}(V_m, V_d) \cdot \frac{1}{\Delta V_d} \tag{41}$$

Finally, a continuous function should be fitted to the discrete $\Delta P\prime_{DSD}(V_m, V_d)$ values to obtain a continuous $P_{DSD}(V_m, V_d)$. It follows that to compare (40) directly with a P_{DSD}, e.g. a P_{DSD} computed from a model, the P_{DSD} must be multiplied by ΔV_d. Here, and for the rest of this work, the daughter size distribution is considered by volume instead of diameter for two reasons. Firstly, the shape of the daughter size distribution is in the literature generally discussed on volume form. Secondly, daughter size distributions by volume are significantly more intuitive. Two drops each at 50% of the volume of the mother drop, would correspond two drops both at $\sim 80\%$ of the diameter of the mother drop. If the daughter size distribution function is desired as a function of diameter, it may be obtained through the fundamental relation given by:

$$P_{DSD}(D_m, D_d)\, dD = P_{DSD}(V_m, V_d)\, dV \tag{42}$$

which is given in e.g. Martínez-Bazán et al. (2010).

3.3. Statistical data treatment

The state of the art single fluid particle experiments are relying on manual and often extremely time consuming approaches. Thus, the statistical treatment of the different parameters are of critical importance. Historically, statistic relevance are attributed experimental investigations with a high number of repetitions, e.g. Maaß and Kraume (2012). Obviously, larger data sets provides an increased precision in the estimates of the quantity investigated, yet this precision is seldom quantified. While the standard deviation provide much information of the nature of the experimental data, models and their validation rely on the statistical mean values. The true mean can be more accurately described by specifying a suitable confidence interval. Moreover, the statistical treatment of the data is seldom discussed in previous works, thus the interpretation of error bars and uncertainties are not clear.

In the following procedure, all of the parameters that the estimated quantities may depend on are assumed constant. The

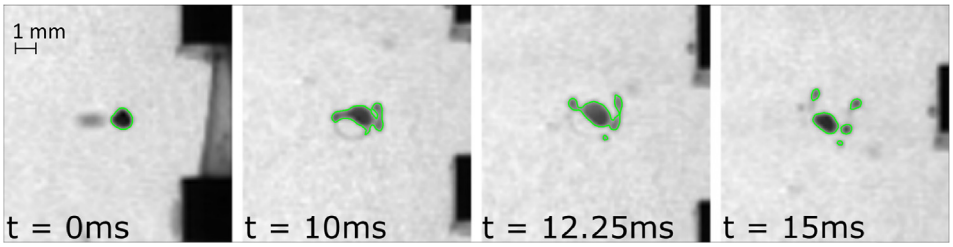

Fig. 4. Breakup resulting several daughters after cascading breakages. The mother drop was 0.89 mm in diameter.

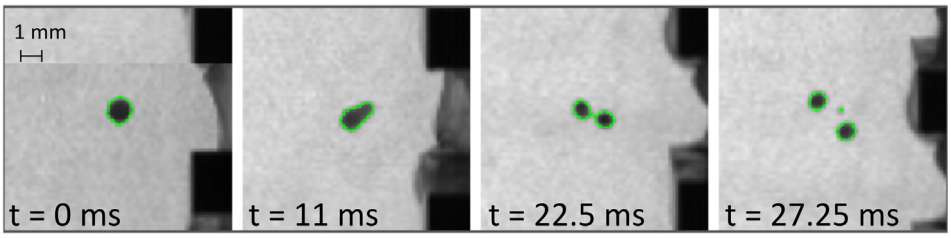

Fig. 5. Breakup sequence resulting two near equal sized daughters and a small drop. The mother drop was 0.99 mm in diameter.

mother drop size, the turbulence level, the interfacial tension, etc., are considered constant for each mother drop size group. The concepts applied can be found in text books on experimental statistics (e.g., Box et al., 2005; Wheeler and Ganji, 2010). Breakage time and the average number of daughter drops are average values, thus the mean, $\bar{x}$, and standard deviation, S, of the data sets may be calculated through the well known relations:

$$\bar{x} = \frac{\sum_{i=1}^{N} x_i}{N} \tag{43}$$

$$S = \left(\frac{\sum_{i=1}^{N} (x_i - \bar{x})^2}{N-1} \right)^{1/2} \tag{44}$$

in which x_i is the value determined in each individual experiment and N is the number of experiments with breakage events. The mean can be assumed to be randomly sampled and belong to a normal distribution of means. That is, the raw data itself may not be normally distributed, but the mean value is assumed to be normally distributed. If the standard deviation in the raw data, often denoted σ, is approximated as S, the standard deviation of the distribution of means are given by $\frac{S}{\sqrt{N}}$. Finally, the $1-\alpha$ confidence interval can be found as

$$\mu = \bar{x} \pm z_{\alpha/2} \frac{S}{\sqrt{N}} \tag{45}$$

In which μ is the true mean value and $z_{\alpha/2}$ is a constant denoting the size of the confidence interval. In a two sided 95%-confidence interval the value of $z_{\alpha/2}$ is $z_{2.5} = 1.96$. In other words, the 95% confidence interval limits, denoted ω, can be computed according to

$$\omega = \pm z_{2.5} \frac{S}{\sqrt{N}} \tag{46}$$

Breakage probability is a binomial distribution as each experiment is either breaking or not. The mean of a binomial distribution is $\mu = N\widehat{P}$ and the standard deviation is

$$\sigma = \sqrt{N\widehat{P}Q} \tag{47}$$

in which N is the number of experiments, including those without breakage events, $\widehat{P}$ is the true probability of breakage occurring and $Q = \widehat{P} - 1$ is the probability of no breakage. At large N and when $\widehat{P}$ is not near either of the extrema 0 or 1, the binomial distribution may be approximated by a normal distribution. Assuming that the calculated experimental probability P^* can be used as an estimate of the true probability $\widehat{P}$ in the standard deviation, the confidence interval of the true number of drops breaking, ΔN_B, can be given as

$$\Delta N_B = NP^* \pm z_{\alpha/2} \frac{\sqrt{NP^*(1-P^*)}}{\sqrt{N}} \tag{48}$$

which, divided by N yields the confidence interval of the breakage probability;

$$\widehat{P} = P^* \pm z_{\alpha/2} \frac{\sqrt{P^*(1-P^*)}}{N} \tag{49}$$

Thus, the probability estimate is computed as

$$P^* = \frac{\text{Number of favorable outcomes}}{\text{Total number of experiments}} \tag{50}$$

and the 95% confidence interval limits as

$$\omega_{P^*} = \pm z_{2.5} \frac{\sqrt{P^*(1-P^*)}}{N} \tag{51}$$

The estimated breakage frequency can be determined according to (4) by the use of the mean value for breakage time and the estimated breakage probability:

$$\bar{b} = \frac{1}{\bar{t}_B} P^* \tag{52}$$

Then, the 95% confidence interval limits can be determined from the confidence interval limits of both the breakage time and the breakage probability. Denoting the interval limits as ω, the expression becomes:

$$\frac{\omega_b}{\bar{b}} = \left[\left(\frac{\omega_{t_B}}{\bar{t}_B} \right)^2 + \left(\frac{\omega_{P^*}}{P^*} \right)^2 \right]^{1/2} \tag{53}$$

Investigating the daughter size distribution function can be done in the same way as the breakage probability. If each daughter size range is considered individually, then the probability that a daughter will appear in the considered daughter size range is binomial. Thus, (50) and (51) can be applied to the results from (40). In this procedure, the sample size N is the number of observed daughters.

In summation, the average breakage time and average number of daughters are computed according to (43), while the standard deviation is computed according to (44). Finally, the confidence interval limits are computed according to (46). The breakage probability and the probability of a daughter appearing in each of the daughter size ranges are computed according to (50), with confidence intervals computed from (51).

4. Results and discussion

4.1. Turbulent quantities

As discussed in Section 3, each experimental run must be associated with the local TDR level in order to validate the model con-

Table 4
TDR level and standard deviation associated with the droplet size groups. The area average velocity of the continuous phase is 1 m/s.

Mother Drop Diameter [mm]	TDR [m^2/s^3]	TDR Breaking [m^2/s^3]	TDR Not Breaking [m^2/s^3]
1.0 ± 0.2	0.2 ± 0.1	0.19 ± 0.09	0.2 ± 0.1
1.48 ± 0.08	0.1 ± 0.1	0.14 ± 0.09	0.1 ± 0.1
1.87 ± 0.05	0.10 ± 0.07	0.09 ± 0.08	0.10 ± 0.07
2.23 ± 0.06	0.09 ± 0.08	0.06 ± 0.07	0.12 ± 0.09

Table 5
TKE level and standard deviation associated with the droplet size groups. The area average velocity of the continuous phase is 1 m/s.

Mother Drop Diameter [mm]	TKE [m^2/s^2]	TKE Breaking [m^2/s^2]	TKE Not Breaking [m^2/s^2]
1.0 ± 0.2	0.02 ± 0.01	0.024 ± 0.009	0.02 ± 0.01
1.48 ± 0.08	0.02 ± 0.01	0.02 ± 0.01	0.02 ± 0.01
1.87 ± 0.05	0.016 ± 0.007	0.015 ± 0.009	0.016 ± 0.008
2.23 ± 0.06	0.01 ± 0.01	0.010 ± 0.008	0.019 ± 0.01

Table 6
TDR level and TKE level, both with 95% confidence intervals. The area average velocity of the continuous phase is 1 m/s.

Mother Drop Diameter [mm]	TDR [m^2/s^3]	TKE [m^2/s^2]
1.0 ± 0.2	0.15 ± 0.03	0.022 ± 0.004
1.48 ± 0.08	0.13 ± 0.02	0.020 ± 0.002
1.87 ± 0.05	0.10 ± 0.02	0.016 ± 0.002
2.23 ± 0.06	0.09 ± 0.02	0.014 ± 0.002

cepts. With the continuous phase area average velocity of 1 m/s, the corresponding TDR characteristic for the mother drop diameter groups, as defined in Table 3, are given in Table 4. Table 4 classifies the TDR level into average of all events, the average of breakage events and the average of events where the drops are not breaking. It can be seen that, within each mother drop size group, the TDR level associated with the breaking drops are comparable to the TDR level associated with non-breaking. Thus, the average TDR level of all events within each mother drop size group are hereafter taken as representative values of the TDR level for the entire group. It should be noted that the largest mother size group has the largest difference in the associated TDR level with breaking and non-breaking drops. The TKE level, found through the same procedure as the TDR level, can be seen in Table 5.

When comparing with models the average turbulence characteristics of each group is of interest, which should be at the highest precision available. Thus, (46) have been employed on the TDR level and the TKE level to obtain the average values and confidence intervals shown in Table 6. While the experimental conditions are clearer shown in Table 4 and Table 5, the values shown in Table 6 are better suited for comparison with models. The increased precision allows to discriminate between the value of 0.15 or 0.2, etc., which lead to significantly different model results.

To investigate the turbulent stress, σ_t, compared to the surface restoring stress, σ_s, a Weber number, i.e. a dimensionless group, may be defined as;

$$\mathrm{We} = \frac{\sigma_t}{\sigma_s} \tag{54}$$

in which the turbulent stress may be approximated through the second order structure function, $\overline{\delta u^2}$, as:

$$\sigma_t \approx \rho_c \overline{\delta u^2}(D_m) \tag{55}$$

where ρ_c is the continuous phase density. In the inertial subrange of turbulence the second order structure function can be approximated through the relation:

$$\overline{\delta u^2}(D_m) \approx \beta(\epsilon D_m)^{2/3} \tag{56}$$

where $\beta = 2$. To account for the entire range of turbulence, the second order structure function may instead be approximated by the expression (30) presented in Section 2.5. Finally, the surface restoring stress can be defined as

$$\sigma_s = \gamma / D_m \tag{57}$$

where γ is the interfacial tension. The Weber numbers of each mother drop size group, as presented in Table 3, are shown in Table 7, which considers both the inertial range and the entire spectrum of turbulence. To compute the entire spectrum as described by Solsvik and Jakobsen (2016a) the TKE is needed, as shown in Table 6. As can be seen from Table 7, the two procedures for determining the turbulent stress results in relatively similar Weber numbers in the current setup. Thus, it is likely that the drop sizes are close to the inertial subrange of turbulence.

Considering that there are breakage events in each mother drop size group, see Table 3, it can be seen that there are breakages for Weber numbers below 1. Some models, like that of Martínez-Bazán et al. (1999a,b, 2010) in Section 2.2, predict no breakage in this case. Thus, it is not possible to compare the model prediction of the breakage time, t_B, the breakage probability, P_B, the average number of daughters, ν, and the daughter size distribution P_{DSD} with the experimental results. It is noted that the model of Martínez-Bazán et al. (1999a,b, 2010) is developed considering very high TDR levels, in the region of $100 - 3000$ m^2/s^3. Thus, it is not unexpected that the model does not accurately predict breakage behavior in the low turbulence level of this study. Nevertheless, the data presented in Table 7 show that breakage takes place also when We < 1. Hence, a breakage model for these fluid and flow conditions should also predict this outcome.

It is noted that investigations of the Weber number should be considered an order of magnitude analysis and not an exact limit. I.e., at large Weber numbers breakage is likely to be prominent, while less common for low Weber numbers. It does not follow that no breakage occurs for We < 1. This can be further illustrated by considering that the expressions for σ_t and σ_s given above are not universal. As an example, the expression for σ_s could have a prefactor of 1, 2, 4 or 6 depending on the derivation, see e.g. Solsvik et al. (2013).

The continuous phase turbulence characteristics are time averaged in this analysis. Thus, the real dynamic interaction between the drop and the turbulent vortex is lost. In transient flows, the TDR level and TKE level experience fluctuations that may be relatively large. In turn, the turbulence level causing breakup may be higher than the averaged values reported in this article. However, experimental investigations of the actual dynamic turbulence-droplet interactions are extremely challenging. An option may be to employ direct numerical simulations, as suggested by Andersson and Helmi (2014). Nevertheless, determining the breakage frequency, b, the average number of daughters, ν, and daughter size distribution, P_{DSD}, based on the local time average turbulence characteristics are certainly of value for development and validation of CFD-PBE simulations. Especially as commonly employed turbulence models, such as Reynolds Averaged Navier–Stokes models, determine time averaged turbulence characteristics. Even with the use of Unsteady Reynolds Averaged Navier–Stokes, the turbulence characteristics are averaged over some time period.

It is noted that the standard deviation within each group of turbulence level in Table 6 is large, thus uncertainty is introduced when employing the average value as the turbulence level. This uncertainty is likely also present in previous experimental studies, where the average TDR level of a finite volume is taken as the turbulence level of all experiments. It is further noted that some

Table 7
Turbulent Weber number associated with the droplet size groups.

Mother drop diameter [mm]	1.0	1.48	1.87	2.23
We - Inertial Range	0.34	0.60	0.75	0.93
We - Entire Spectrum	0.35	0.68	0.84	1.04

Table 8
Selected cascade breakage times taken from regressional fit of the data in Solsvik and Jakobsen (2015).

Mother drop diameter	1 mm	1.5 mm	2 mm
Petroleum	~ 10 ms	~ 20 ms	~ 35 ms
Octanol	~ 20 ms	~ 40 ms	~ 60 ms

authors, e.g. Foroushan and Jakobsen (2020), have investigated the breakage phenomenon through an instability analysis. That is, instead of considering a single turbulent vortex-droplet interaction, the breakage event is considered to be due to a series of interactions. While this treatment leads to an increased complexity, it might be the correct interpretation of the turbulence-droplet interaction. If that is the case, the determined turbulence characteristics in this study might not be sufficient to explain the relation between the turbulence level and the breakage phenomenon.

4.2. Breakage time

Only a limited number of experimental single droplet studies report breakage time, t_B, fewer yet investigate the impact of mother drop size, D_m. Currently, the effect of mother drop size on average breakage time is not sufficiently validated by single drop experiments. A selection of representative values from the study of Solsvik and Jakobsen (2015) are presented in Table 8. In their investigation of breakup in a stirred tank, they found that, for a given stirrer speed and oil, the breakage time is increasing with increasing mother drop size. This trend is consistent with the models presented in Section 2. On the other hand, when Maaß and Kraume (2012) investigated channel flow around a stirrer blade, they did not observe a clear trend. Some representative values from the latter study are given in Table 9. Interestingly, they found that the longest average breakage times were for the smallest drop sizes, contrary to the model concepts in Section 2 and to the results of Solsvik and Jakobsen (2015). Maaß and Kraume (2012) employed the initial breakage definition with a slight modification. In their procedure, the breakage event start instance was taken as the instance of the drop passing the stirrer blade. However, this instance does not necessarily correspond to the instance of the beginning of a breakage, see Section 3.1. Due to a recirculating flow pattern behind the stirrer blade, a drop could pass the stirrer blade and stay spherical, before breaking at a later time instance. Maaß and Kraume (2012) recognized the weakness themselves. Based on the interpreted videos, it was stated the phenomenon of recirculating drops was more frequent in experiments on the smallest drop sizes, which was given as the explanation for why the smallest drop sizes had the longest average breakage times. Maaß and Kraume (2012) claimed that the distribution of breakage time was a β-distribution. Thus, the problem of the average value being saturated by long breakage time was avoided by utilizing the peak of the β-distribution as the breakage time measurement. This breakage time estimate did follow the trend of increasing breakage time with increasing mother drop size. In summary, there is a general belief that, for a given system, an increase in mother drop size should increase the breakage time. As noted in Section 1, it is challenging with direct and quantitative comparison between different experimental studies due to differences in the experimental setup, such as flow condition, dispersed phase and breakage event definition.

In this study, the average breakage time of each mother drop group, see Table 3, has been determined for both the initial breakage definition and the cascade breakage definition. The results are shown in Fig. 6 and Fig. 7, respectively. As expected, due to the cascade breakage definition including the time after the initial breakage definition, the cascade breakage times are significantly longer than the initial breakage times.

By both the breakage event definitions, the average breakage time show a trend of increasing breakage time with increasing mother drop diameter. This is consistent with the cascade breakage results of Solsvik and Jakobsen (2015), although the breakage times of this study are longer. The difference in the determined breakage time may be dependent on mainly two factors. First, the discrepancy with the petroleum results may be partly due to different system properties when working with different oils. Secondly, Solsvik and Jakobsen (2015) used a stirrer with an volume average TDR level at 1 m^2/s^3, which is higher than the values seen in Table 6 by a factor of approximately 5 to 10. Additionally, the TDR level in the breakup region near the impeller blade is likely much higher than 1 m^2/s^3 (Solsvik and Jakobsen, 2015), as the TDR level is not uniform in the stirrer. Thus, some of the difference may be due to the turbulent intensity of the setup in this study being significantly lower than that of Solsvik and Jakobsen (2015). This may have an impact on the results, as it is likely that the breakage time decreases with increasing turbulence levels, as shown by e.g. Andersson and Andersson (2006a) and consistent with (11) and (20) of Section 2.

In order to compare the model of Coulaloglou and Tavlarides (1977) with the experimental results of this study, (11) is computed. First, the mother drop size and TDR level is taken from Table 6. Then, the parameter c_2 is fitted to a linear equation, with the constant term set to zero. The procedure is performed in MATLAB by using the fit function and the "poly1" method. This yields the value of c_2 as 1.54 when employing the initial breakage definition. This is close to the value determined by Maaß and Kraume (2012), who found the value of c_2 to be ~ 1.1. Their breakage definition was similar to the initial breakage definition. When employing the cascade breakage definition instead, the value of c_2 was found to be 2.39. Coulaloglou and Tavlarides (1977) found the original value of c_2 to be ~ 2.98, when comparing with data from dense dispersion experiments. As such, neither of the parameter values are very different from previously determined values.

Additionally, the data is compared to the Coulaloglou and Tavlarides model adaption of Solsvik and Jakobsen (2016a), which is valid for the entire range of turbulence. Fitting the parameter c_4 in (28) using the same procedure as described above, yields the values of c_4 as 2.30 and 3.57 for the initial and cascade breakage definitions, respectively. The value of c_4 is determined experimentally for the first time. However, Solsvik and Jakobsen (2016a) showed that the value of c_4 is not equal to the value of c_2, which is in line with the present results.

From the Fig. 6 it can be seen that the predictions of the model of Coulaloglou and Tavlarides (1977) and the model adaption of Solsvik and Jakobsen (2016a), plotted as triangles and circles respectively, are very similar. Additionally, the model predictions are in reasonable agreement with the experimentally determined initial breakage time. However, the predicted breakage time of the largest mother drop size group is significantly lower than the average value of the experimental results. While the predicted breakage time is within the standard deviation, it is outside the 95% confidence interval. This mother drop size group had a large difference in the turbulence level associated with breakage events and non breakage events. Thus, it is possible that the discrepancy between model prediction and experimental value of the largest

Table 9
Selected average breakage times from Maaß and Kraume (2012).

Mother drop diameter	0.65 mm	1.0 mm	2.0 mm	3.0 mm
Toluene	19.7 ms	12.4 ms	14.3 ms	16.1 ms
Mother drop diameter	0.535 mm	1.0 mm	1.9 mm	3.1 mm
Petroleum	34.0 ms	16.0 ms	13.9 ms	16.6 ms

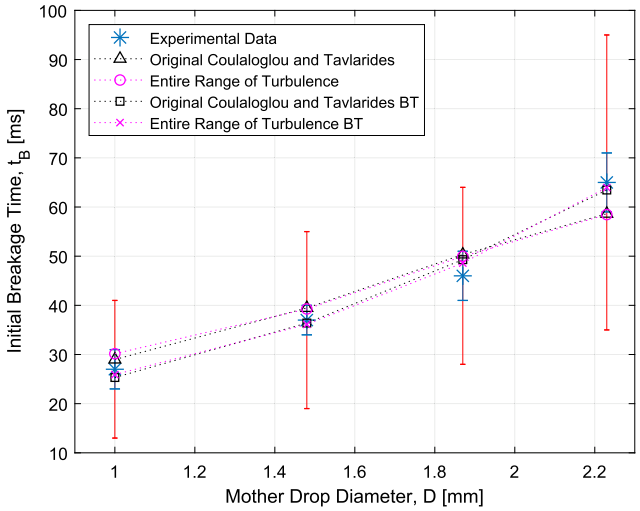

Fig. 6. Average breakage time considering the initial breakage definition plotted with 95%-confidence interval in blue and standard deviation in red. The confidence interval is computed according to (46). The model predictions are computed using (11) by Coulaloglou and Tavlarides (1977) and (28) by Solsvik and Jakobsen (2016a). BT denotes model predictions utilizing the turbulence associated with breakage events only.

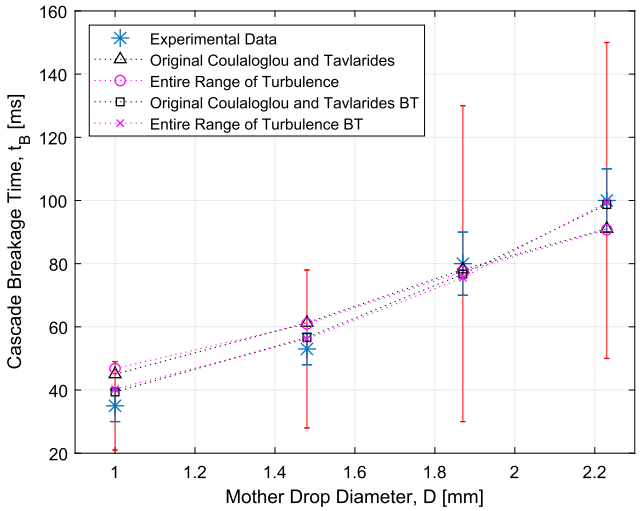

Fig. 7. Average breakage time considering the cascade breakage definition plotted with 95%-confidence interval in blue and standard deviation in red. The confidence interval is computed according to (46). The model predictions are computed using (11) by Coulaloglou and Tavlarides (1977) and (28) by Solsvik and Jakobsen (2016a). BT denotes model predictions utilizing the turbulence associated with breakage events only.

mother drop size group is partly due to the procedure employed when associating turbulence level with the mother drop size groups. In light of this, an additional model fitting is performed in which the turbulence level associated with breakage events only is employed, instead of the average turbulence level of all events. As such, different values for c_2 and c_4 are obtained. Considering the initial breakage definition values, the value of c_2 is found to be 1.46 and the value of c_4 is 2.15. The resulting model predictions are plotted as squares and exes in Fig. 6. As can be seen from the figure, this provides a much better fit to every point on the graph.

For the breakage time determined considering the cascade breakage definition, Fig. 7, the predictions of the model of Coulaloglou and Tavlarides (1977) and the model adaption of Solsvik and Jakobsen (2016a) are plotted as triangles and circles. It can be seen from the figure that the model predictions are similar to each other. However, the model predictions are in general less accurate than for the initial breakage time, as seen in Fig. 6. In the same procedure as above, the model parameters are fitted to the turbulence level associated with the breakage events only. The following model predictions are plotted as squares and exes. It can be seen from the figure, that these model predictions represent a better parameter estimation. In this procedure, the value of c_2 is determined to be 2.26 and the value of c_4 is found to be 3.35.

Unfortunately, it is not clear how the turbulence level associated with the breakage events only can be associated with the breakage probability. The determination of breakage probability requires consideration of both the events with breakage and the events in which breakage does not occur. While it is intuitive that the breakage time is dependent on the turbulence level causing breakage, a consistent model for the breakage frequency uses only one turbulence level, i.e. the same turbulence value for both breakage time and breakage probability. Thus, the turbulence level associated with the breakage events only is not further employed in this study. The good fit obtained when parameter fitting with this turbulence level may be an indication of a need for improvement of the procedure, which may warrant further study.

4.3. Breakage probability

The breakage probabilities determined from (50) are shown in Fig. 8, with the 95%-confidence interval included in red. The standard deviation from (47) is not shown, as the breakage probability is determined from the number of drops breaking divided by the number of experiments. Thus, the standard deviation does not provide additional insight into the probability investigated. As can be seen from Fig. 8, the breakage probability is increasing monotonously with droplet diameter. This general trend is in agreement with previous experimental investigations. Both Galinat et al. (2005, 2007), for an orifice flow, and Ashar et al. (2018), for a stirred tank, showed that there exists a critical Weber number below which there is no breakage and that the probability increases monotonously with increasing Weber number. In their experimental setups, increasing the Weber number translates to either increasing the diameter of the mother drop or increasing the average flow conditions, i.e. continuous phase volume flow or stirrer speed. Maaß and Kraume (2012) reported the same trend; for petroleum the breakage probability was ~ 0.55 and ~ 0.8 for mother drop diameter of 1 mm and 2 mm, respectively, while the breakage probabilities for toluene drops of the same size were ~ 0.6 and ~ 0.75.

The predicted breakage probability of the models of Coulaloglou and Tavlarides (1977), given by (9), and Solsvik and Jakobsen (2016a), given by (29), is also shown in Fig. 8. Following the same

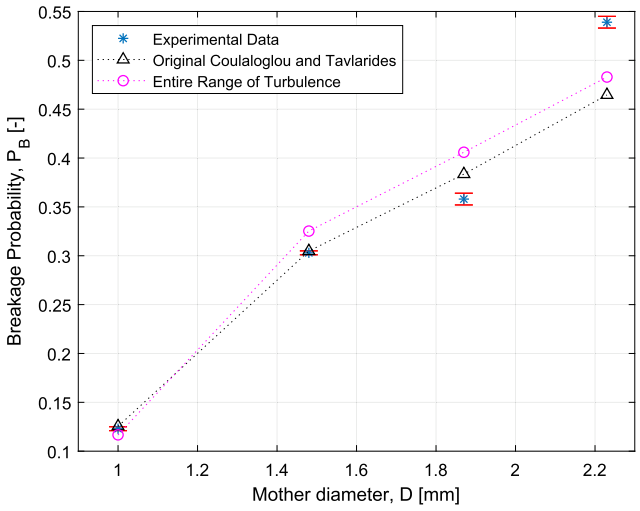

Fig. 8. Breakage probability plotted in blue. The 95%-confidence interval, computed according to (49), is plotted in red. The model predictions are computed using (9) by Coulaloglou and Tavlarides (1977) and (29) by Solsvik and Jakobsen (2016a).

procedure as in the previous section, the parameter c_1 is fitted in MATLAB, yielding the value 0.59. Previously, Maaß and Kraume (2012) found the value of c_1 to be 0.39, while Coulaloglou and Tavlarides (1977) found the value to be 0.106. The fitted value of c_5 in (29) is 1.25. The value of c_5 is determined experimentally for the first time. However, Solsvik and Jakobsen (2016a) showed that the value of c_5 is not equal to the value of c_1. It can be seen from Fig. 8 that the model predictions are reasonable for the two smallest mother drop sizes, but less accurate for the two largest ones. The reason for this behavior is not clear.

4.4. Breakage frequency function

Even though the breakage frequency, b, is what is used in modeling the breakage death and breakage birth terms of the PBE, the only single droplet study previously investigating this value is the study by Maaß and Kraume (2012). In general, their results suggests that when increasing the mother drop size, the breakage frequency trends to rapidly increase at first, before going through a maximum value and slowly decrease. This was assumed to happen under the same turbulence conditions. Some representative breakage frequency values from the study by Maaß and Kraume (2012) are $\sim 175\ s^{-1}$ and $\sim 75\ s^{-1}$ for toluene mother drop sizes of 1 mm and 2 mm, respectively, and for petroleum the breakage frequency was determined as $\sim 120\ s^{-1}$ and $\sim 80\ s^{-1}$.

The breakage frequency estimated in this study, computed using (52), can be seen in Fig. 9. Compared to that of Maaß and Kraume (2012), the breakage frequency is significantly lower. Which is expected, as the breakage time of this study is longer, Section 4.2, and the breakage probability is lower, Section 4.3. This can likely be attributed to the different flow conditions and fluid properties employed in this study.

From Fig. 9 it can also be seen that the breakage frequency based on the cascade breakage time is lower than the frequency based on the initial breakage time, which is due to the cascade breakage time by definition being larger than the initial breakage time. Furthermore, it appears that the breakage frequency is increasing at first, before it stabilizes or slightly declines, which in turn is a similar to the trend reported by Maaß and Kraume (2012). Considering the initial breakage definition, the experimental results are also in reasonable agreement with the model predictions of Coulaloglou and Tavlarides (1977) and the model predictions of Solsvik and Jakobsen (2016a).

Although the breakage time and breakage probability estimates of the largest mother drop size group was both predicted inaccurately, the breakage frequency of this size group is well predicted. Of course, this may be a coincidence. Nevertheless, the different experimental breakage frequency data are well predicted by the models. A possible reason for the high accuracy is the association of the local turbulence level with the breakage event instead of a volume average approach. From the data based on the local turbulence level approach, the disruptive turbulent force is accurately modeled and the resulting model prediction is close to the measured values. This result highlights the importance of associating the turbulence level with local values, even for a low gradient system as employed in this study.

4.5. Average number of daughters

Similarly to the breakage time, the average number of daughter drops produced from a breakage event, ν, is significantly dependent on the breakage definition employed. In the current study, the number of daughters for the initial breakage definition was always determined to be two. I.e. due to the high frame rate used in the experiments, it was always possible to identify a frame in which a drop was broken into two daughters, before possibly continuing the breakage process. Solsvik et al. (2016a) suggested that the number of daughters of the initial breakage would tend to two as the framerate increased, which appears to be supported by the data presented in this work.

In the cascade breakage definition the average number of daughters depend on the mother drop diameter, as seen in Fig. 10. Both the average number of daughters and the standard deviation is increasing with increasing mother drop diameter. Interestingly, the number is significantly larger than the binary outcome determined from the initial breakage definition, even for the smallest mother drop diameters. The trend of this study correspond to that of the previous investigations of Galinat et al. (2005, 2007) and Ashar et al. (2018). Even though these authors report significantly higher turbulence levels in their setups,

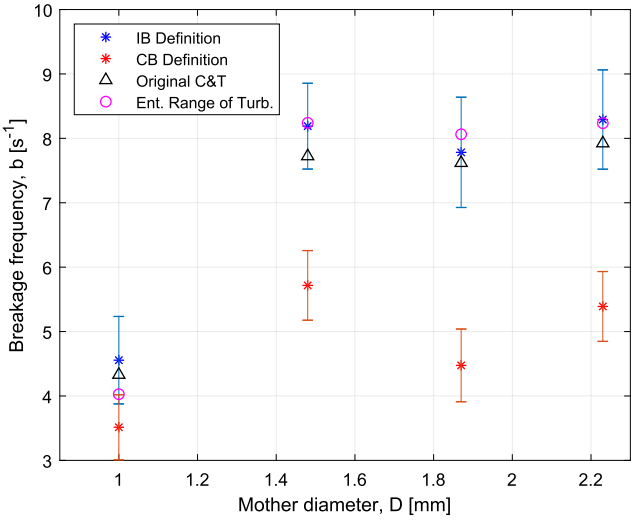

Fig. 9. Breakage frequency, computed using (52), plotted with an estimated 95%-confidence interval, computed using (53). "IB definition" and "CB definition" denotes the breakage frequency determined with breakage time from the initial breakage definition and the cascade breakage definition, respectively. The model predictions are computed using (12) by Coulaloglou and Tavlarides (1977), denoted as "Original C&T", and according to the procedure of Solsvik and Jakobsen (2016a), as presented in 2.5, denoted as "Ent. Range of Turb.".

Galinat et al. (2005, 2007) found the average number daughters to be ~ 3 to ~ 8 and Ashar et al. (2018) found it to be ~ 3 to ~ 7. Galinat et al. (2005) also reported a high standard deviation, which is increasing with increasing mother drop size.

In the models available in the literature, the average number of daughter drops produced upon breakage is a constant which must be given before any simulations are performed. While the binary breakage assumption appears to hold for the initial breakage framework, it does not hold for the cascade breakage framework. If the cascade breakage definition is advantageous in order to describe the breakage phenomenon, then the breakage models should determine the average number of daughters as a function dependent on the mother drop size, the local flow conditions and the system properties. Additionally, the models should be able to predict non-integer values for average number of daughters.

The underlying probability distribution of daughter numbers is of interest in order to elucidate the resulting average number of daughters and the high standard deviation. Fig. 11 shows the probability of daughter number for each mother drop diameter. For the smallest mother drop diameter binary, tertiary and quaternary breakage are the most frequent outcome and there are no events of seven or more daughters. As the mother drop increases, cases with higher number of daughters appear and the curve is flattened while binary and tertiary breakage are still the most common outcome of any breakage event. The same trends, i.e. distribution of daughter number dependent on mother drop size, are previously reported by Solsvik and Jakobsen (2015) and Solsvik et al. (2016a). In those studies, all but the smallest drop sizes have an even distribution in the range 2 to 11 daughter drops.

4.6. Daughter size distribution

In contrast to the breakage frequency and the daughter number, the daughter size distribution function is not only an average value, but a function for each mother drop size. The shape of the daughter size distribution is usually considered from a theoretical point of view with the assumption of binary breakage. Depending the strategy employed in model derivation, the daughter size distribution can be considered to have a variety of shapes. Considered on volume form, some of the common shapes include bell-, U-, bimodal- or uniformly-shaped. The discussion of the shape is significantly influenced by the binary breakage assumption and few alternative formulations exists. One alternative is the model by Diemer and Olson (2002), in which any average number of daughters is possible and the daughters are most likely to be near equal in size. Other models have been proposed by Han et al. (2011, 2013, 2015) and Solsvik et al. (2016b), in which the daughter number may be 2, 3 or 4. Also for these models, the daughters are most likely to be near equal in size.

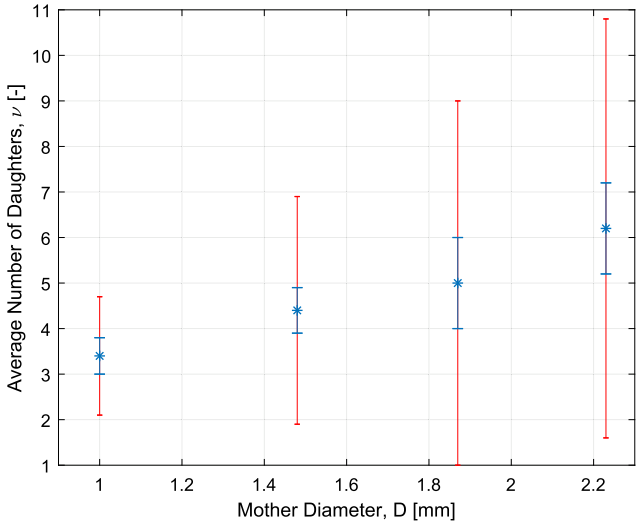

Fig. 10. Cascade breakage average number of daughters with a 95%-confidence interval in blue, computed using (46), and standard deviation in red.

As with the breakage time and average number of daughters, the choice of breakage definition greatly impacts the experimentally determined daughter size distribution. First, the initial breakage definition is considered, and the resulting daughter size distributions, calculated according to (40), is shown in Fig. 12. The smallest mother drop size group, Fig. 12a has the highest likelihood of equal breakage, but otherwise a near uniform distribution. Then the two middle size groups, Fig. 12b and c, have nearly uniform distributions. Finally, the largest mother drop size group, Fig. 12d, show that it is more likely with a small and a large drop, i.e. a U-shape. Generalized, the trend in the daughter size distribution, as the mother drop size increases, appears to be a uniform distribution with a weak preference of equal breakage, then a uniform distribution before eventually obtaining a relatively small preference for the U-shape. Also from the Fig. 12, it can be seen that for every mother drop size group there is no daughter size that is not apparent. The biggest difference is found for the U-shape of the largest mother drop size group, Fig. 12d, where the least common outcome is $\sim 6\%$ and the most common outcome is $\sim 19\%$.

The model predictions from (14) by Coulaloglou and Tavlarides (1977) are included in the Fig. 12 for completeness. According to the procedure in Section 3.2, the model predicted daughter size distribution function is computed from (41). The model framework assumes two daughters, which coincides with the experimental results. However, the assumption of equal sized breakage dominating is not accurate. While equal sized breakage obviously is present to obtain a uniform distribution, it is not more frequent than unequal sized breakage. As such, the model is not accurately predicting any of the experimentally determined distributions. The best fit is obtained for the shape of the smallest mother drop size group and becomes worse for increasing mother drop size. This behavior is expected based on the discussion above.

The resulting daughter size distributions of the cascade breakage definition, Fig. 13, are very different from the initial breakage definition. For each mother drop size group, there is a large probability of obtaining the smallest class of drops. This probability is the lowest for the smallest mother drop size group and increases as the mother drop size increases, which is also related to an increase in the average number of daughters. Such a large probability of small drops are previously not reported in literature(e.g. Galinat et al., 2005, 2007; Maaß et al., 2007). From the investigated videos, it appears that breaking drops often deforms into a dumbbell shape, with two soon-to-be daughter drops connected by a thin thread. As the breakup progresses, this results in two larger drops and a number of smaller drops originating from the thread. In some cases, the larger daughter drops undergo the process again, yielding even more small drops.

As for the initial breakage definition, the model predictions from (14) by Coulaloglou and Tavlarides (1977) are included in the Fig. 13. For the cascade breakage definition, the discrepancy between the assumed binary breakage of the model and the experimental data is large. As such, the model fails to predict the experimental data. This is due to the small size of many of the daughter drops, which is considered unlikely to be produced by the model prediction. Thus, a different breakage model is needed to determine the daughter size distribution function in the cascade breakage event definition. Currently, there are no existing models that predict multiple unequal sized breakage events. However, such a model is needed in order to predict the current experimental data.

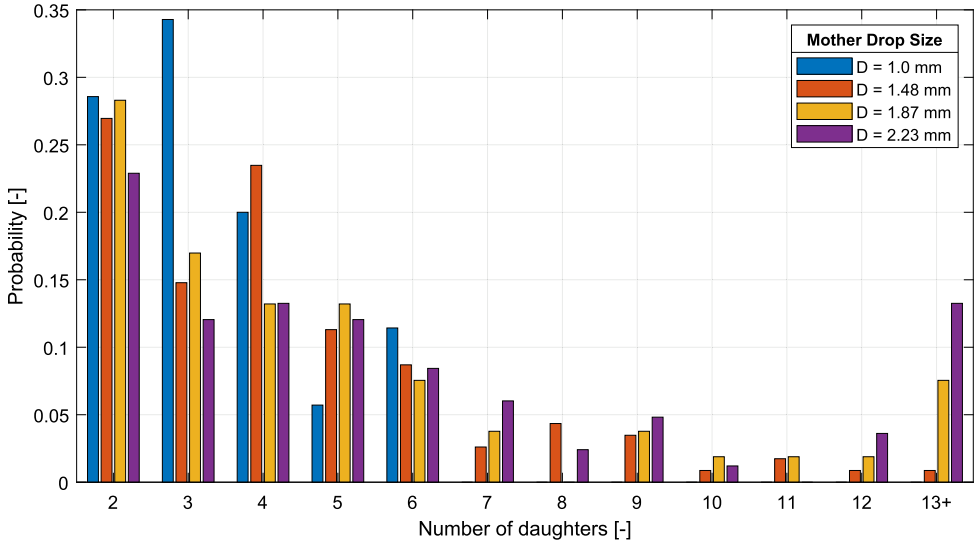

Fig. 11. Distribution of number of daughters in the cascade breakage definition.

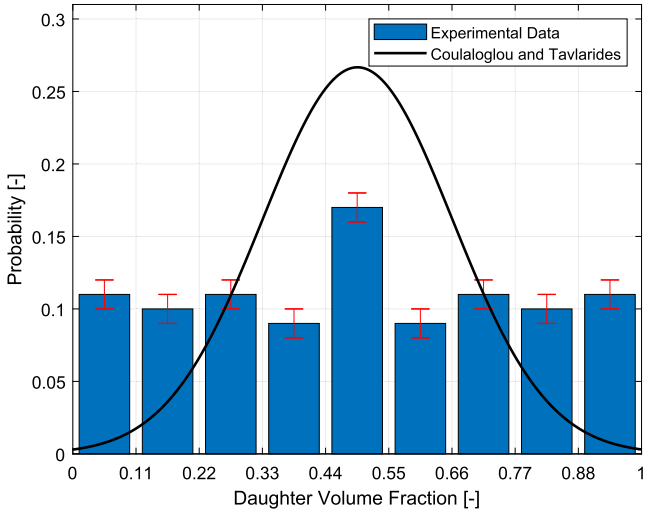

(a) Mother drop size group of diameter 1.0 mm

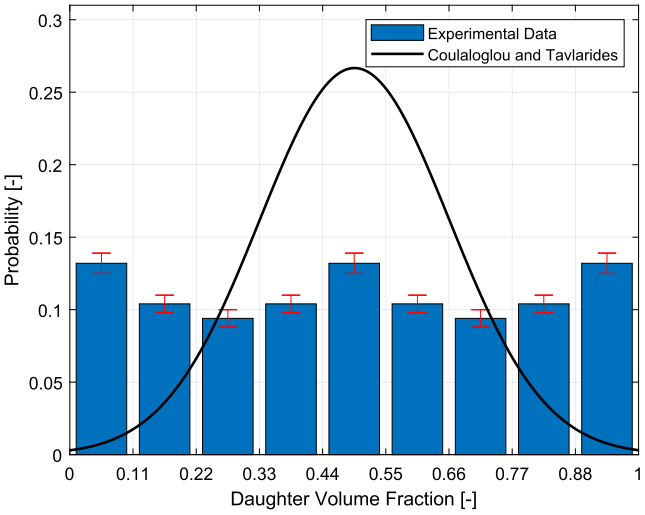

(c) Mother drop size group of diameter 1.87 mm

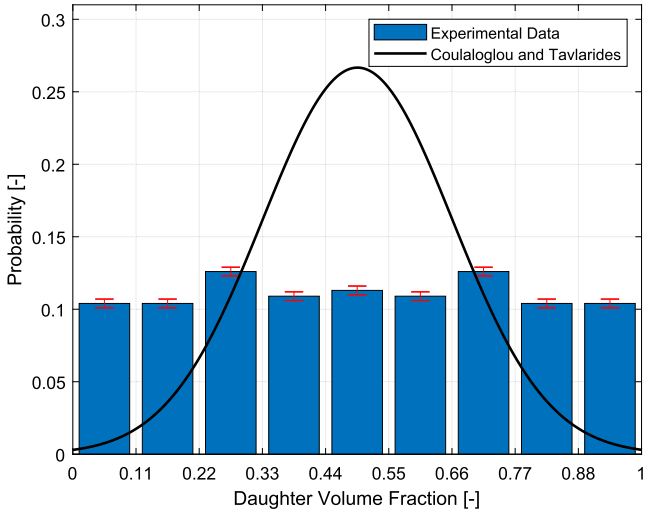

(b) Mother drop size group of diameter 1.48 mm

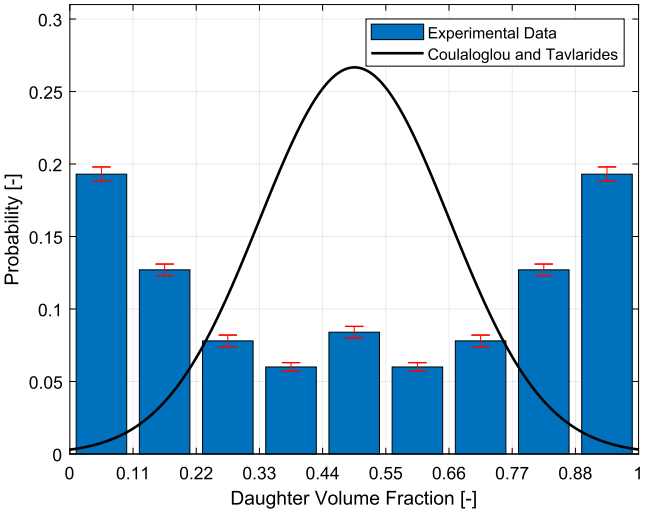

(d) Mother drop size group of diameter 2.23 mm

Fig. 12. Daughter size distributions, calculated according to (40) and utilizing the initial breakage definition. Confidence interval calculated from (51). The model predictions are computed from (14) by Coulaloglou and Tavlarides (1977), in accordance with (41).

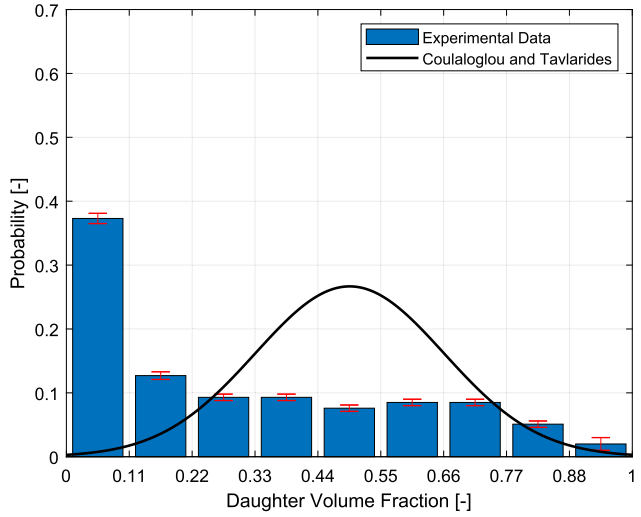

(a) Mother drop size group of diameter 1.0 mm

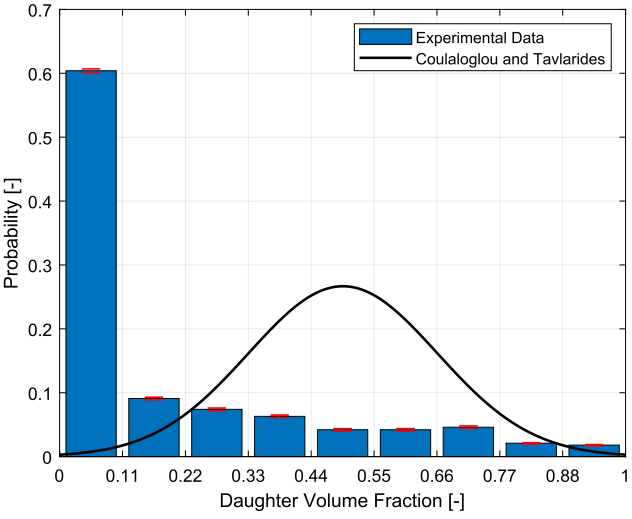

(c) Mother drop size group of diameter 1.87 mm

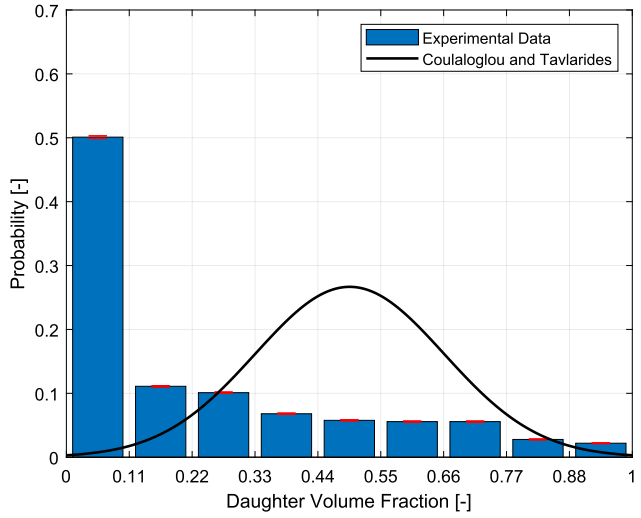

(b) Mother drop size group of diameter 1.48 mm

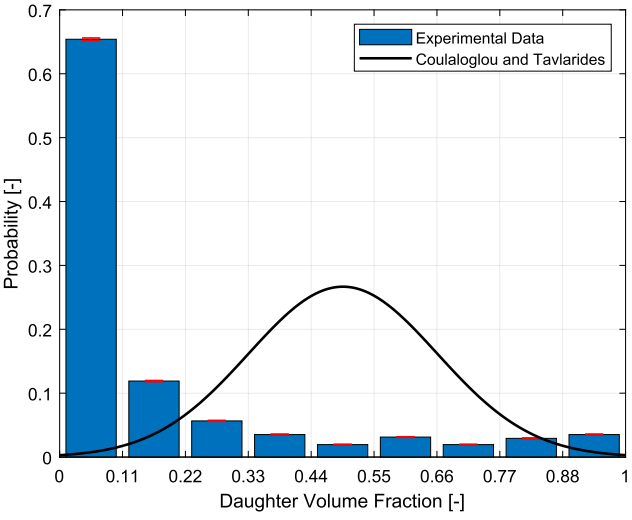

(d) Mother drop size group of diameter 2.23 mm

Fig. 13. Daughter size distributions, calculated according to (40) and utilizing the cascade breakage definition. Confidence interval calculated from (51). The model predictions are computed from (14) by Coulaloglou and Tavlarides (1977), in accordance with (41).

Neither the initial breakage definition, nor the cascade breakage definition has one general daughter size distribution curve valid for all of the mother drop size groups. Considering the cascade breakage definition the probability of the smallest drops is increasing significantly with increasing mother drop size. Which is obvious considering that the average number of daughters is increasing significantly, thus the number of smaller drops increase simultaneously. Contrary to these experimental data, breakage models give the shape of the daughter size distribution before any simulations are performed. However, the shape of the daughter size distribution is likely dependent on the mother drop size, the local flow conditions and the system properties. A predictive breakage model should account for these dependencies.

It is noted that the currently employed procedure for determining the daughter size distribution is different from previous investigations. Maaß et al. (2007) grouped the breakage events by the number of daughters produced upon breakage. As such, one daughter size distribution function is determined for binary breakage, one for tertiary breakage, and so on. Thus, Maaß et al. (2007) obtained unique daughter size distribution functions for each integer value of the average number of daughters. This approach could be used to validate models such as Han et al. (2011, 2013, 2015), where unique equal size daughter size distribution functions are available for the average number of daughters as 2, 3 or 4. However, for a given system, different daughter numbers and sizes may be the outcome of different breakage events, i.e. there is a presence of binary breakage, tertiary breakage, quartary breakage and so on, each with a different daughter size distribution. It is not clear how the different daughter size distribution functions of Maaß et al. (2007) should be combined to obtain the daughter size distribution function corresponding to the average number of daughters.

In the present study, all daughter drops produced from breakage events of the given mother drop size group is considered collectively, regardless of whether a given daughter originated from a binary breakage, tertiary breakage, etc. This results in one daughter size distribution per mother drop size group. As such, the presence of different outcomes of the breakage event is incorporated in the determined distribution function. The current procedure is similar to that of Galinat et al. (2005), although they did not use single droplet experiments for this determination.

4.7. Statistical treatment

The experimental data might be subject to a number of sources of error. This may include experimental lab procedure, data processing or assumptions, among others. Random errors contributes to the standard deviation in the experimental data and increases the size of the confidence interval. Systematic errors are present regardless of the individual experiment and usually considered not to be randomly applied. For example, if the thread of oil between two soon-to-be daughter drops is very thin, the thread might not be visible by the camera and the breakage assumed to have ended. Subsequently, some breakage times may be predicted to be shorter than the true value, but none are predicted to be longer. As such, it mostly impacts the determined mean value and not the standard deviation. If the impact of systematic errors is large enough, the true mean may fall outside the confidence interval from the statistical analysis. It follows that the employment of the statistical analysis is no guarantee that the true mean value is within the confidence interval. Furthermore, performing a very large number of experiments in order to obtain a small confidence interval is, in most experimental studies, not beneficial. At a certain number of experiments, the statistical precision is close to the total uncertainty arising from the experimental procedure, thus repeating the experiment under the same conditions, e.g. drop size, oil type and flow conditions, provides limited additional information. Instead, other aspects of the breakage phenomenon should be investigated.

Before investigating the determined statistical uncertainty, a short discussion on the uncertainties in the experimental procedure is required. While the models are defined as point values, the experimental data is taken from a volume. Ideally, the experimental data should be determined as representative for points, which would translate to a very small experimental volumes. This is practically impossible on several accounts. First, there are practical limitations. Due to fluctuations in the channel flow and in the droplet generation channel, the droplets will have an almost random horizontal motion. Thus, the droplets are traveling along different trajectories despite having nearly equal initial conditions. The amount of experiments needed to be able to validate every single point would be extremely large. This is even further complicated by the randomness of the turbulence level, which means that breakage can happen at different vertical positions, even for droplets transported along the same trajectory. Second, the association of each breakage with a single location is disputable, as each experimental breakage event clearly has a duration in which the droplet or droplets are transported. While it appears to be natural to associate the breakage with the position at the breakage event start instance, this is not determined from the PBE model framework considered. In summation, the procedure of considering a larger volume is a necessary simplification. It does, however, include some uncertainty which cannot be quantified.

4.7.1. Breakage time

From the figure showing the initial breakage time, Fig. 6, and the figure showing the cascade breakage time, Fig. 7, it can be seen that the standard deviation in breakage time for each mother drop size group is significant. This is expected, as each mother drop within each group might be slightly different in size, break in different positions, i.e. turbulence level, or experience different instantaneous turbulent conditions. On the other hand, the confidence intervals are fairly small. As the trends are similar for the initial breakage definition and the cascade breakage definition, only the cascade breakage definition will be considered in the following discussion. The standard deviation in the breakage time, as seen in Fig. 7, is $40\%, 47\%, 63\%$ and 50% when given in relative values. In contrast, the 95% confidence intervals are $14\%, 9\%, 13\%$ and 10%. Thus, the mean values are more precisely determined statistically, than what appears to be the case when only considering the standard deviation. Furthermore, it does not appear beneficial to determine the statistical uncertainty below $\sim 10-15\%$ with the current procedure, when considering the large variation in TDR level and the uncertainties discussed in the start of this section. As such, additional experiments under the same conditions are not required. This decision is also influenced by the feasibility of improving the confidence intervals.

From (46) it can be seen that the size of the confidence interval limits is dependent on the standard deviation and the number of experiments. When performing experiments, the standard deviation approaches a constant value. When this constant value is obtained, the confidence interval is only dependent on the factor $N^{-1/2}$, which has a diminishing effect on the confidence interval limits as N increases. For example, at $N = 30$, the value of $N^{-1/2}$ is ~ 0.18, while at $N = 40$, the value of $N^{-1/2}$ is ~ 0.16. Assuming that the standard deviation was constant at 30 experiments, the ten additional experiments from 30 to 40 experiments only shortened the confidence interval limits by $\sim 2\%$ of the value of the standard deviation. This is shown graphically in Fig. 14, which shows the mean value, standard deviation and confidence interval of the cascade breakage time plotted as a function of the number of experiments performed for the 1.48 mm mother drop size group. As can be seen from the figure, the mean value appears to be relatively stable after 20 experiments. However, it is possible to improve the standard deviation by performing approximately 10 additional experiments. From this point onward, the standard deviation is near constant. The confidence interval can still be improved with additional experiments, but this does have a diminishing effect per experiment performed, as explained above. The mean value does experience some oscillation after 20 experiments, but this is within even the final confidence interval limits.

4.7.2. Breakage probability

Breakage probability, Fig. 8, is the only function in the expression for breakage frequency that requires data of the drops not breaking. As such, the experimental value is determined from a larger set of data than e.g. breakage time. It is therefore expected that the confidence intervals for the breakage probability are smaller

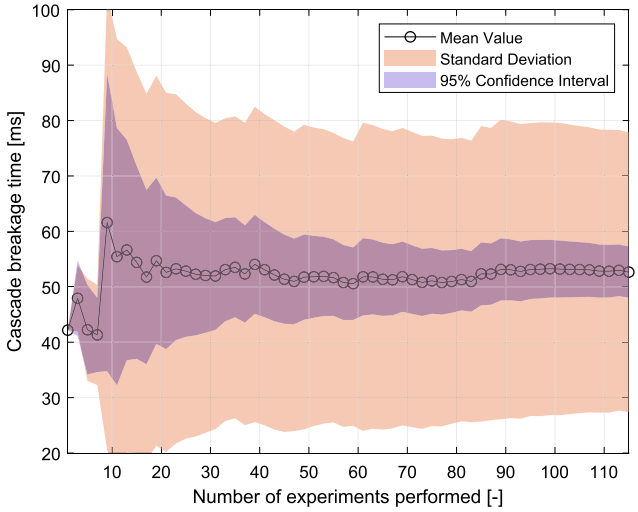

Fig. 14. Plot of the cascade breakage time of the 1.48 mm mother drop size group from Table 3. It shows the development in determined mean value, standard deviation and confidence interval of the cascade breakage time, by the number of experiments performed. The values are calculated for every two experiments from the first until the final 115.

than the confidence intervals for the breakage times, i.e. the breakage probability is more precise from a purely statistical point of view. The small confidence interval is a strong indication that the determined breakage probability is unlikely to change significantly if an increased number of experiments are performed.

4.7.3. Breakage frequency

The breakage frequency is not determined directly, rather it is determined from the breakage time and breakage probability. The same is true for the uncertainty in the breakage frequency. It is directly related to the uncertainty in the breakage time and breakage probability by (53). As such, it is not necessary with an additional discussion of the uncertainty in the breakage frequency when the uncertainty in both breakage time and breakage probability have been discussed extensively.

4.7.4. Average number of daughters

In the Fig. 10, showing the average number of daughters, there are sizeable standard deviations and subsequently large confidence intervals. Which, from Fig. 11 is reasonable, as there is a rather flat distribution for most of the mother drop sizes. The standard deviation in a flat distribution is always large. Thus, it follows that additional experiments are not likely to significantly improve the statistical precision of the average number of daughters. Instead, different aspects of the breakage phenomenon should be investigated.

4.7.5. Daughter size distribution

The daughter size distribution is a special case, as it is a distribution for each mother drop size group instead of an average value. Due to the presentation of the distribution in bins, as in Fig. 12 and in Fig. 13, there are two precisions to consider; the number of bins and the confidence interval of each bin. As such, when deciding whether to continue with the same experimental conditions or change, one must also consider whether the number of bins is sufficient. As for the breakage time, breakage probability and daughter number, the choice of precision must be weighted against the error sources in the experimental work.

In comparison to the initial breakage, the cascade breakage daughter sizes have increased precision due to the daughters often being observed in a near spherical shape, as the sequence of breakages normally has ended. For the cases where the cascade ends in many daughters, the determination of the size of the initial breakage daughters is very challenging, as the initial breakage daughters often are severely deformed in the few video frames they are visible. In short, in the current experimental procedure, the initial breakage definition is not optimal to determine the daughter size distribution when successive breakages are common. On the other hand, the procedure of scaled volume, as outlined in Section 4.9, is accurate if the initial breakage daughter drops of a single breakage can be assumed to deform in a similar manner. Unfortunately, based on the investigated videos, this is a course, and not quantified, assumption.

From the Fig. 13, showing the daughter size distribution when considering the cascade breakage definition, it can be seen that the confidence intervals are very small. With the nine bins used in this study, the statistical precision cannot be meaningfully improved by additional experiments. With this number of bins, near equal and equal size breakage end up in the same bin and the size of each bin is $\sim 11\%$ of the mother drop size, a reasonable precision considering the uncertainties and error sources discussed above.

4.8. Experimental setup design

A survey on the design process of the current experimental facility is included here to elucidate the main challenges in designing the facility. The facility was designed to obtain experimental data for increased physical understanding of the breakage process and validation of breakage models in the PBE framework. A systematic study of previous experimental facilities, both within droplet breakage experiments and homogeneous turbulence, was performed. Three main points were identified as critical in order to obtain the required quality and quantity of data.

1. Observation of the entire breakage event
   The entire breakup should be continuously observed for two reasons. First, this ensures that the breakage definitions are correctly applied. Second, the obtained experimental results cover all of the necessary data to validate the breakage time, t_B, the breakage probability, P_B, the average number of daughters, ν, and the daughter size distribution P_{DSD}. Thus ensuring a coherent dataset that may be used for validate breakage models.
2. Known local turbulence level
   From Section 2 it can be seen that the breakage models rely on the impact of the local turbulence level. Thus, in order to associate the breakages with a representative turbulence characteristic, the facility should have known local turbulence levels. Additionally, the accuracy of the determined turbulence level is increased with low gradients in the turbulence level. In an ideal facility for investigating turbulent breakage, the breakup would happen in homogeneous and isotropic turbulence. However, 3D isotropic turbulence is not experimentally feasible. In setups with 2D isotropic turbulence, e.g. after static mixer (Azizi and Al Taweel, 2011) or near oscillating grids (Shy et al., 1997; Yan et al., 2007), the turbulence level is rapidly decaying in the third direction. The setups also has high shear forces in the area generating the turbulence. In conclusion, it is challenging to inject a droplet into a region of sufficiently high turbulence level. As an added challenge, the facility would be challenging to automate.
3. Repeatable and reproducible
   In order to obtain enough data within a reasonable time, the experimental runs should be easily repeatable. Firstly, the facility operation should be automated. In order to obtain this automation, it is critical to ensure a reliable injection of dispersed phase drops. The criterion of repeatability also means that designs which require substantial cleaning between one or few experiments are disregarded. Likewise, designs in which the continuous phase cannot be reused, which will lead to a very large consumption of the continuous phase, are disregarded.

Considering only points 1 and 2 above, it would be beneficial to also observe the breakage in the third dimension. However, this is challenging due to increased complexity in the facility design, automation and image analysis. In turn, this significantly increases the time required to perform each experiment. However, it is noted that observation of all three dimensions has been performed, for gas bubbles in a stirred tank, by Krakau and Kraume (2019).

Some important lessons has been learned from the operation of the facility. First, the facility is designed as a loop with a 1000 liter tank functioning as both continuous phase storage and gravity separator, separating the small oil droplets from the water. While the separation works as intended, the inlet generated air bubbles. Despite the size of the tank, these bubbles reentered the loop and interfered with the image analysis. The situation was remedied by installing a partially holed plate near the inlet of the tank, which acts as a momentum breaker and redistributes the inlet flow over a larger area.

In order to create the continuous phase flow, the setup uses a positive displacement pump. This gives a reasonably stable mass flow, but also give rise to pressure fluctuations. These fluctuations manly interfere with the size of the injected droplets, giving rise to a fluctuation in the generated droplet size. The problem can be mitigated by geometric considerations in the design of the facility, as some flow patterns dampen pressure fluctuations. In this particular case, a sudden expansion of the cross sectional area was installed before the droplet generation section. Additional solutions include installation of a pressure dampener, although no commercial pressure dampeners are available at such low pressure levels. A simple solution is to implement a T-section which allows a volume of air to be compressed. Additionally, an adjustment that may mitigate pressure fluctuations is to implement a coiled tube in the loop. As the flow is going through the coil, the pressure fluctuations are dampened by the oscillation of the coil.

The droplet size is also influenced by the surface finish of the cannula tip area, where a courser surface finish yields a larger fluctuation in the droplet size generated. Due to this dependence on surface finish, less fluctuation in droplet size is experienced with regular cleaning of the cannula tip.

Finally, still water is an excellent breeding grounds of algae. In particular when high intensity light is present, as is the case in high speed imaging facilities. Thus, it is critical to have a procedure for easy cleaning of the setup, as well as easy exchanging of water. As algae settles on the walls, the ability to drain the experimental section of water is highly advantageous to avoid algae buildup on the wall during periods in which the facility is not in use.

4.9. Image analysis algorithm

As mentioned in Section 3.1, the procedure employed in this paper differentiate from the algorithm presented in Herø et al. (2019) on the determination of daughter drop sizes. Daughter drops are often recorded with irregular shapes. Thus, calculating the diameter from the projected area, assuming the drop to be spherical, and calculating the volume from this diameter can lead to a total volume which is larger than the volume of the original mother drop. In a few extreme cases, this estimated volume is 100% larger than the mother drop volume in the initial breakage definition, and 50% larger in the cascade breakage definition. In order to determine the daughter sizes, the daughter drops are associated with a fraction, which is subsequently associated to the mother drop size. In Herø et al. (2019), it was suggested obtain this fraction from the projected area of each daughter drop divided by the total projected area of daughter drops. In this work the daughter drop size is estimated by a volume fraction instead, as volume scales differently than area and it is the volume that is to be conserved. For each daughter drop, the projected area is assumed circular and a diameter is calculated, then this diameter is used to estimate the volume of the corresponding daughter drop, assuming it to be spherical. From this, the volume fraction of a particular daughter drop relative to all the daughter drops is found. Subsequently, the daughter drop volume is approximated as the same fraction of the mother drop volume.

The determination of the breakage event start instance is essentially an attempt to determine the instance of a single critical turbulent vortex-drop interaction, or the start of this interaction. The application of the described procedure is elucidated here in order to increase the readers understanding of the video interpretation process. The procedure is based on determining the start instance of the oscillation in the projected area, normal to the camera, that is related to the breakage event. In practice, the determination of the breakage event start is performed after the determination that a breakage event has taken place. From the instance of fragmentation, i.e. when two drops can be discerned, one can move backwards in time on the video until a near spherical drop is detected. In this procedure, oscillations denote changes to the projected drop area where the drop is significantly deformed from spherical, i.e. becoming ellipsoidal or irregularly shaped. Thus, very small perturbations of near spherical mothers are not considered. As an example, consider a low complexity breakage event in which a non-oscillating mother drop starts to deform and break. Such a breakage event can be seen in Fig. 15. The figure shows the mother drop projected area, normalized by the initial mother drop projected area, frame by frame leading up to a breakage of the drop. The arrow indicates the determined breakage event start instance. The small changes in projected area before the arrow are not considered to be related to the breakage event. These oscillations are assumed either to be due to very small perturbations in the projected area of the drop, artifacts from the image analysis or a combination of the two effects.

However, in many breakage events, the mother drop is going through several smaller oscillations before undergoing a significantly larger deformation directly before breakage. Subsequently, the determination of the instance of one vortex-drop interaction

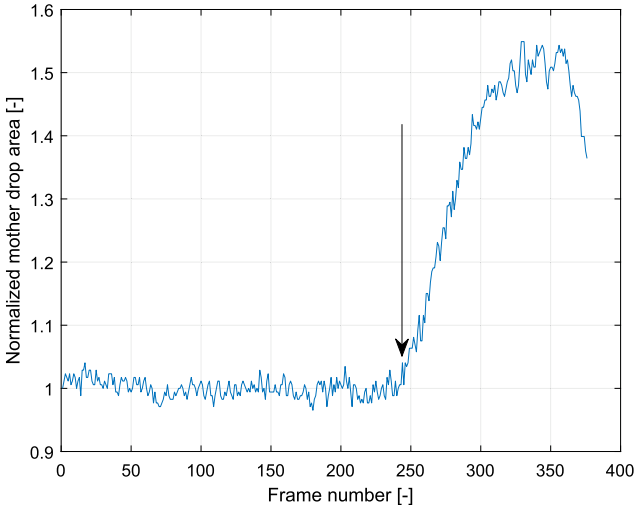

Fig. 15. A breakage event with only one oscillation before breakage. The arrow denotes the instance of the start of breakage. The mother drop area is normalized by the area of the mother drop in the first frame.

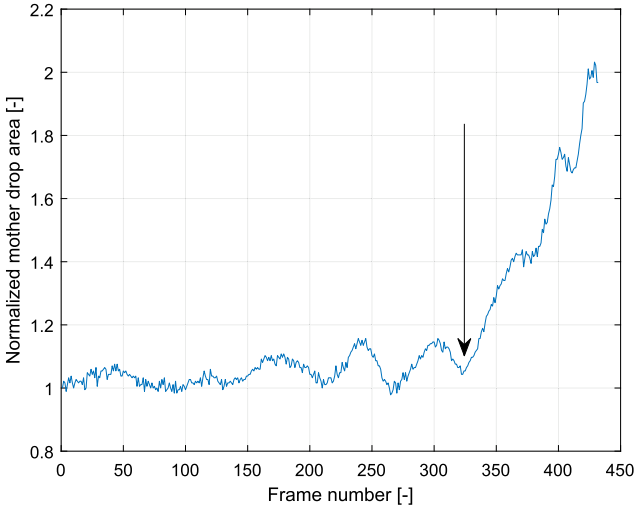

Fig. 16. A breakage event with several oscillations before breakage. The arrow denotes the instance of the start of breakage. The mother drop area is normalized by the area of the mother drop in the first frame.

is less clear. Dampened oscillations are not considered part of the vortex-drop interaction, as the energy appears to be dissipated. Thus, another vortex-drop interaction is considered responsible for the breakage event. An example of such an event may be seen in Fig. 16. The first oscillations are seemingly dampened, hence they are considered unrelated to the breakage event, as the drop undergoes a significantly larger deformation during the breakage event. This large deformation is assumed to be due to a single vortex-droplet interaction, therefore the breakage event start instance is assumed to be at the instance before this deformation. In Fig. 16 this instance is indicated by the arrow. This breakage event start instance is also an instance of spherical mother drop, which ideally, but not always, has been spherical for several frames. It is noted that the drop in Fig. 16 is visibly oscillating from around frame 150 until the breakage event takes place.

5. Conclusions

Single octanol drop breakage experiments in turbulent flow have been performed. The droplets were inserted into a channel flow and the following breakage events were captured by high speed cameras. The videos obtained were interpreted by adopting both the initial breakage definition and cascade breakage definition. Furthermore, the design of the channel allows for breakage events to occur in a turbulent flow with low gradients.

The impact of mother drop size on the breakage phenomenon were investigated. While the flow considered is characterized by a level of turbulence that is lower than for comparable breakage investigations previously reported in literature, the results show similar trends. With a specified constant flow rate in the channel, an increase in mother drop size induces an increase in breakage time and breakage probability. Considering the initial breakage definition, the number of daughter drops was always two and the daughter size distribution was close to uniform. However, when considering the cascade breakage definition, the number of daughters increased with increasing mother drop size. The corresponding daughter size distributions had a large probability of very small drops which only increase with increased number of daughters. Due to the various shapes of the daughter size distribution for the different mother drop size groups, breakage models should determine the shape of the daughter size distribution dependent on the mother drop size, the local flow conditions and the system properties. For the cascade breakage definition, also the average number of daughters should be determined in this way.

A statistical analysis have been employed in order to quantify the quality of the data and to address the requirement of statistically valid data. In particular, the analysis show that adequate statistical precision could be obtained, in this study, with as few as 35 to 50 breakage events. Due to the uncertainties inherent in the experimental procedure, further increasing the statistical precision, i.e. increase the number of investigated events, is not cost effective. Instead, investigations should focus on obtaining data with different system properties or, if possible, increase the accuracy and precision of the experimental procedure. Furthermore, the statistical analysis show that, for this study, the breakage probability is determined with lower uncertainty than the breakage time, while the average number of daughters is less precise than the daughter size distribution functions.

Each breakage event is associated with a local turbulence level. As data from different experiments are combined in order to obtain the average breakage time, the breakage probability, the average number of daughter and the daughter size distributions, the resulting average turbulence level is relevant to the events considered. Furthermore, the turbulence level has a quantified standard deviation that can be used to describe the uncertainty of the procedure.

In general, more single drop breakage data from experiments is still needed to elucidate the breakage phenomenon. In the experimental facility, different fluid and system properties might be investigated. For example, investigating different continuous flow velocities, i.e. turbulence level, or different oils. In addition, efforts should be made into determining whether the initial breakage definition or the cascade breakage definition best describes the breakage phenomenon. Finally, the data should be used for discriminating between breakage models.

Each mother drop size group has a different turbulent kinetic energy dissipation rate levels associated with it, and the difference in turbulence level between two events can be large. This may have an impact on the results and subsequently the investigated trends. Thus, the impact of mother drop size might warrant further study. Possibly, the problem could be mitigated by investigating a smaller volume, such that the breakages happen under less varying conditions. However, decreasing the volume would lead to an increase in the needed number of experiments, as each volume would need enough data to be statistically relevant.

CRediT authorship contribution statement

Eirik H. Herø: Conceptualization, Methodology, Software, Formal analysis, Investigation, Data curation, Writing - original draft. **Nicolas La Forgia:** Conceptualization, Methodology, Software, Investigation, Writing - review & editing. **Jannike Solsvik:** Conceptualization, Writing - review & editing. **Hugo A. Jakobsen:** Conceptualization, Writing - review & editing, Supervision.

Declaration of Competing Interest

The authors declare that they have no known competing financial interests or personal relationships that could have appeared to influence the work reported in this paper.

Acknowledgment

This work was carried out as a part of SUBPRO, a research based innovation center within Subsea Production and Processing. The authors gratefully acknowledge the financial support from SUBPRO, which is financed by the Research Council of Norway, major industry partners, and NTNU.

References

Andersson, R., Andersson, B., 2006a. On the breakup of fluid particles in turbulent flows. AIChE J. 52 (6), 2020–2030. https://doi.org/10.1002/aic.10831. http://doi.wiley.com/10.1002/aic.10831.

Andersson, R., Andersson, B., 2006b. Modeling the breakup of fluid particles in turbulent flows. AIChE J. 52 (6), 2031–2038. https://doi.org/10.1002/aic.10832. http://doi.wiley.com/10.1002/aic.10832. arXiv:arXiv:1402.6991v1.

Andersson, R., Helmi, A., 2014. Computational fluid dynamics simulation of fluid particle fragmentation in turbulent flows. Appl. Math. Model. 38 (17–18), 4186–4196. https://doi.org/10.1016/j.apm.2014.01.005.

Ashar, M., Arlov, D., Carlsson, F., Innings, F., Andersson, R., 2018. Single droplet breakup in a rotor-stator mixer. Chem. Eng. Sci. 181, 186–198. https://doi.org/10.1016/j.ces.2018.02.021. https://linkinghub.elsevier.com/retrieve/pii/S0009250918300836.

Azizi, F., Al Taweel, A.M., 2011. Hydrodynamics of liquid flow through screens and screen-type static mixers. Chem. Eng. Commun. 198 (5), 726–742. https://doi.org/10.1080/00986445.2011.532748.

Box, G.E.P., Hunter, J.S., Hunter, W.G., 2005. Statistics for Experimenters. Wiley-Interscience, Hoboken.

Coulaloglou, C.A., Tavlarides, L.L., 1977. Description of interaction processes in agitated liquid-liquid dispersions. Chem. Eng. Sci. 32 (11), 1289–1297. https://doi.org/10.1016/0009-2509(77)85023-9.

Diemer, R., Olson, J., 2002. A moment methodology for coagulation and breakage problems: Part 3—generalized daughter distribution functions. Chem. Eng. Sci. 57 (19), 4187–4198. https://doi.org/10.1016/S0009-2509(02)00366-4. https://www.sciencedirect.com/science/article/pii/S0009250902003664.

Eastwood, C.D., Armi, L., Lasheras, J.C., 2004. The breakup of immiscible fluids in turbulent flows. J. Fluid Mech. 502, 309–333. https://doi.org/10.1017/S0022112003007730.

Foroushan, H.K., Jakobsen, H.A., 2020. On the dynamics of fluid particle breakage induced by hydrodynamic instabilities: a review of modelling approaches. Chem. Eng. Sci. 219, 115575. https://doi.org/10.1016/j.ces.2020.115575. https://linkinghub.elsevier.com/retrieve/pii/S000925092030107X.

Galinat, S., Masbernat, O., Guiraud, P., Dalmazzone, C., Noïk, C., 2005. Drop break-up in turbulent pipe flow downstream of a restriction. Chem. Eng. Sci. 60 (23), 6511–6528. https://doi.org/10.1016/j.ces.2005.05.012.

Galinat, S., Torres, L.G., Masbernat, O., Guiraud, P., Risso, F., Dalmazzone, C., Noik, C., 2007. Breakup of a drop in a liquid-liquid pipe flow through an orifice. AIChE J. 53 (1), 56–68. https://doi.org/10.1002/aic.11055. http://doi.wiley.com/10.1002/aic.11055. arXiv:arXiv:1402.6991v1.

Håkansson, A., Trägårdh, C., Bergenståhl, B., 2009. Dynamic simulation of emulsion formation in a high pressure homogenizer. Chem. Eng. Sci. 64 (12), 2915–2925. https://doi.org/10.1016/j.ces.2009.03.034. https://linkinghub.elsevier.com/retrieve/pii/S0009250909002164.

Han, L., Luo, H., Liu, Y., 2011. A theoretical model for droplet breakup in turbulent dispersions. Chem. Eng. Sci. 66 (4), 766–776. https://doi.org/10.1016/J.CES.2010.11.041. https://www.sciencedirect.com/science/article/pii/S0009250910007037.

Han, L., Gong, S., Li, Y., Ai, Q., Luo, H., Liu, Z., Liu, Y., 2013. A novel theoretical model of breakage rate and daughter size distribution for droplet in turbulent flows. Chem. Eng. Sci. 102, 186–199. https://doi.org/10.1016/J.CES.2013.06.046. https://www.sciencedirect.com/science/article/pii/S0009250913004697.

Han, L., Gong, S., Ding, Y., Fu, J., Gao, N., Luo, H., 2015. Consideration of low viscous droplet breakage in the framework of the wide energy spectrum and the multiple fragments. AIChE J. 61 (7), 2147–2168. https://doi.org/10.1002/aic.14830. http://doi.wiley.com/10.1002/aic.14830.

Herø, E.H., Forgia, N.L., Solsvik, J., Jakobsen, H.A., 2019. Determination of breakage parameters in turbulent fluid-fluid breakage. Chem. Eng. Technol. 42 (4), 903–909. https://doi.org/10.1002/ceat.201800610.

Jakobsen, H.A., 2014. Chemical reactor modeling. Springer, Berlin.

Karimi, M., Andersson, R., 2018. An exploratory study on fluid particles breakup rate models for the entire spectrum of turbulent energy. Chem. Eng. Sci. 192, 850–863. https://doi.org/10.1016/J.CES.2018.08.016. https://www.sciencedirect.com/science/article/pii/S0009250918305852?via%3Dihub.

Karimi, M., Andersson, R., 2019. Dual mechanism model for fluid particle breakup in the entire turbulent spectrum. AIChE J., e16600 https://doi.org/10.1002/aic.16600.

Konno, M., Aoki, M., Saito, S., 1983. Scale effect on breakup process in liquid-liquid agitated tanks. J. Chem. Eng. Jpn. 16 (4), 312–319. https://doi.org/10.1252/jcej.16.312.

Krakau, F., Kraume, M., 2019. Three-dimensional observation of single air bubble breakup in a stirred tank. Chem. Eng. Technol. https://doi.org/10.1002/ceat.201900033. ceat.201900033, https://onlinelibrary.wiley.com/doi/abs/10.1002/ceat.201900033.

La Forgia, N., Herø, E.H., Solsvik, J., Jakobsen, H.A., 2018. Dissipation rate estimation in a rectangular shaped test section with periodic structure at the walls. Chem. Eng. Sci. 195, 159–178. https://doi.org/10.1016/j.ces.2018.11.039.

Lasheras, J., Eastwood, C.D., Martínez-Bazán, C., Montañés, J., 2002. A review of statistical models for the break-up of an immiscible fluid immersed into a fully developed turbulent flow. Int. J. Multiph. Flow 28 (2), 247–278. https://doi.org/10.1016/S0301-9322(01)00046-5.

Liao, Y., Lucas, D., 2009. A literature review of theoretical models for drop and bubble breakup in turbulent dispersions. Chem. Eng. Sci. 64 (15), 3389–3406. https://doi.org/10.1016/j.ces.2009.04.026.

Liao, Y., Oertel, R., Kriebitzsch, S., Schlegel, F., Lucas, D., 2018. A discrete population balance equation for binary breakage. Int. J. Numer. Meth. Fluids 87 (4), 202–215. https://doi.org/10.1002/fld.4491. http://doi.wiley.com/10.1002/fld.4491.

Luo, H., Svendsen, H.F., 1996. Theoretical model for drop and bubble breakup in turbulent dispersions. AIChE J. 42 (5), 1225–1233. https://doi.org/10.1002/aic.690420505. http://www.ncbi.nlm.nih.gov/pubmed/19947509 http://doi.wiley.com/10.1002/aic.690420505.

Maaß, S., Kraume, M., 2012. Determination of breakage rates using single drop experiments. Chem. Eng. Sci. 70, 146–164. https://doi.org/10.1016/j.ces.2011.08.027.

Maaß, S., Gäbler, A., Zaccone, A., Paschedag, A.R., Kraume, M., 2007. Experimental investigations and modelling of breakage phenomena in stirred liquid/liquid systems. Chem. Eng. Res. Des. 85 (5 A), 703–709. https://doi.org/10.1205/cherd06187.

Maaß, S., Wollny, S., Sperling, R., Kraume, M., 2009. Numerical and experimental analysis of particle strain and breakage in turbulent dispersions. Chem. Eng. Res. Des. 87 (4), 565–572. https://doi.org/10.1016/j.cherd.2009.01.002. https://linkinghub.elsevier.com/retrieve/pii/S0263876209000057.

Maaß, S., Buscher, S., Hermann, S., Kraume, M., 2011. Analysis of particle strain in stirred bioreactors by drop breakage investigations. Biotechnol. J. 6 (8), 979–992. https://doi.org/10.1002/biot.201100161.

Martínez-Bazán, C., Montañés, J.L., Lasheras, J.C., 1999. On the breakup of an air bubble injected into a fully developed turbulent flow. Part 1. Breakup frequency. J. Fluid Mech. 401, S0022112099006680. doi:10.1017/S0022112099006680. http://www.journals.cambridge.org/abstract_S0022112099006680.

Martínez-Bazán, C., Montañés, J.L., Lasheras, J.C., 1999. On the breakup of an air bubble injected into a fully developed turbulent flow. Part 2. Size PDF of the resulting daughter bubbles. J. Fluid Mech. 401, S0022112099006692. doi:10.1017/S0022112099006692. http://www.journals.cambridge.org/abstract_S0022112099006692 http://www.journals.cambridge.org/abstract_S0022112099006680.

Martínez-Bazán, C., Rodríguez-Rodríguez, J., Deane, G.B., Montaes, J.L., Lasheras, J.C., 2010. Considerations on bubble fragmentation models. J. Fluid Mech. 661, 159–177. https://doi.org/10.1017/S0022112010003186.

Mitre, J., Takahashi, R., Ribeiro, C., Lage, P., 2010. Analysis of breakage and coalescence models for bubble columns. Chem. Eng. Sci. 65 (23), 6089–6100. https://doi.org/10.1016/J.CES.2010.08.023. https://www.sciencedirect.com/science/article/pii/S0009250910004902.

Nachtigall, S., Zedel, D., Kraume, M., 2016. Analysis of drop deformation dynamics in turbulent flow. Chin. J. Chem. Eng. 24 (2), 264–277. https://doi.org/10.1016/j.cjche.2015.06.003.

Ramkrishna, D., 2000. Population balances: Theory and applications to particulate systems in engineering. Academic Press, San Diego.

Revuelta, A., Rodríguez-Rodríguez, J., Martínez-Bazán, C., 2006. Bubble break-up in a straining flow at finite Reynolds numbers. J. Fluid Mech. 551, 175–184. https://doi.org/10.1017/S0022112005008505. http://www.journals.cambridge.org/abstract_S0022112005008505.

Shy, S.S., Tang, C.Y., Fann, S.Y., 1997. A nearly isotropic turbulence generated by a pair of vibrating grids. Exp. Thermal Fluid Sci. 14 (3), 251–262. https://doi.org/10.1016/S0894-1777(96)00111-2.

Solsvik, J., 2017. Turbulence modeling in the wide energy spectrum: explicit formulas for Reynolds number dependent energy spectrum parameters. Eur. J. Mech. B. Fluids 61, 170–176. https://doi.org/10.1016/j.euromechflu.2016.10.011. https://linkinghub.elsevier.com/retrieve/pii/S0997754616303211.

Solsvik, J., Jakobsen, H.A., 2015. Single drop breakup experiments in stirred liquid-liquid tank. Chem. Eng. Sci. 131, 219–234. https://doi.org/10.1016/j.ces.2015.03.059.

Solsvik, J., Jakobsen, H.A., 2016a. Development of fluid particle breakup and coalescence closure models for the complete energy spectrum of isotropic turbulence. Ind. Eng. Chem. Res. 55 (5), 1449–1460. https://doi.org/10.1021/acs.iecr.5b04077. http://pubs.acs.org/doi/10.1021/acs.iecr.5b04077.

Solsvik, J., Jakobsen, H.A., 2016b. A review of the statistical turbulence theory required extending the population balance closure models to the entire spectrum of turbulence. AIChE J. 62 (5), 1795–1820. https://doi.org/10.1002/aic.15128. http://doi.wiley.com/10.1002/aic.15128.

Solsvik, J., Tangen, S., Jakobsen, H.A., 2013. On the constitutive equations for fluid particle breakage. Rev. Chem. Eng. 29 (5), 241–356. https://doi.org/10.1515/revce-2013-0009.

Solsvik, J., Maaß, S., Jakobsen, H.A., 2016a. Definition of the single drop breakup event. Ind. Eng. Chem. Res. 55 (10), 2872–2882. https://doi.org/10.1021/acs.iecr.6b00591.

Solsvik, J., Skjervold, V.T., Han, L., Luo, H., Jakobsen, H.A., 2016b. A theoretical study on drop breakup modeling in turbulent flows: The inertial subrange versus the entire spectrum of isotropic turbulence. Chem. Eng. Sci. 149, 249–265. https://doi.org/10.1016/J.CES.2016.04.037. https://www.sciencedirect.com/science/article/pii/S0009250916301968#bib11.

Solsvik, J., Skjervold, V.T., Jakobsen, H.A., 2017. A bubble breakage model for finite Reynolds number flows. J. Dispersion Sci. Technol. 38 (7), 973–978. https://doi.org/10.1080/01932691.2016.1216440. https://www.tandfonline.com/doi/full/10.1080/01932691.2016.1216440.

Tsouris, C., Tavlarides, L.L., 1994. Breakage and coalescence models for drops in turbulent dispersions. AIChE J. 40 (3), 395–406. https://doi.org/10.1002/aic.690400303. http://doi.wiley.com/10.1002/aic.690400303.

Vankova, N., Tcholakova, S., Denkov, N.D., Vulchev, V.D., Danner, T., 2007. Emulsification in turbulent flow: 2. Breakage rate constants. J. Colloid Interface Sci. 313 (2), 612–629. https://doi.org/10.1016/j.jcis.2007.04.064. https://linkinghub.elsevier.com/retrieve/pii/S0021979707005413.

Wheeler, A.J., Ganji, A.R., 2010. Introduction to Engineering Experimentation. Pearson Higher Education, Upper Saddle River.

Xing, C., Wang, T., Guo, K., Wang, J., 2015. A unified theoretical model for breakup of bubbles and droplets in turbulent flows. AIChE J. 61 (4), 1391–1403. https://doi.org/10.1002/aic.14709. http://doi.wiley.com/10.1002/aic.14709.

Yan, J., Cheng, N.S., Tang, H.W., Tan, S.K., 2007. Oscillating-grid turbulence and its applications: a review. J. Hydraul. Res. 45 (1), 26–32. https://doi.org/10.1080/00221686.2007.9521740.

Zaccone, A., Gäbler, A., Maaß, S., Marchisio, D., Kraume, M., 2007. Drop breakage in liquid–liquid stirred dispersions: Modelling of single drop breakage. Chem. Eng. Sci. 62 (22), 6297–6307. https://doi.org/10.1016/J.CES.2007.07.026. https://www.sciencedirect.com/science/article/pii/S000925090700526X#bib6.